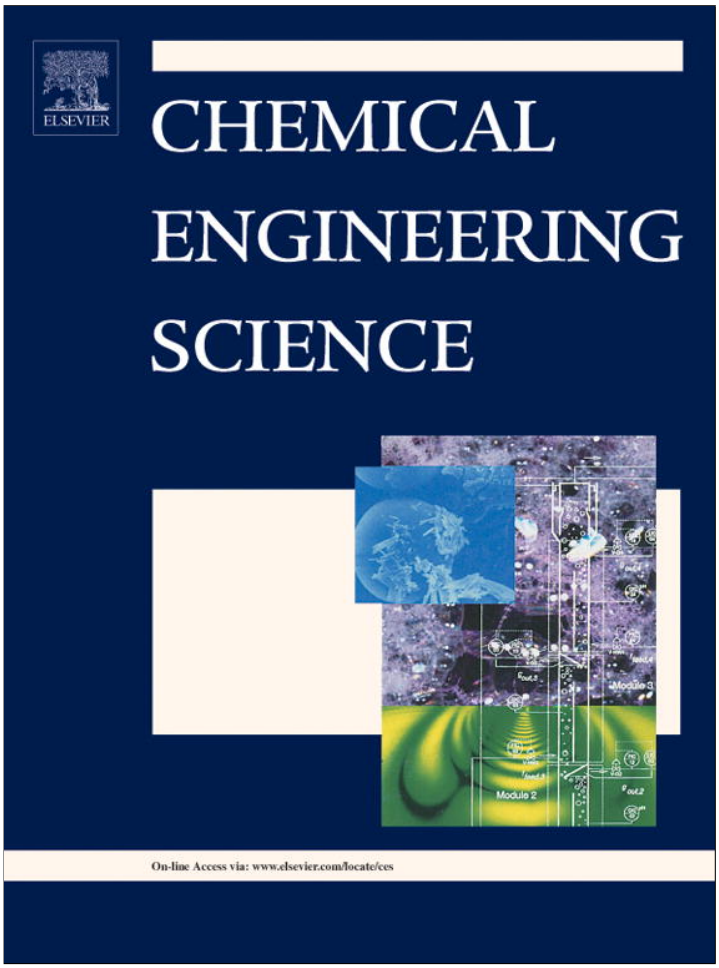

(This is a sample cover image for this issue. The actual cover is not yet available at this time.)

Chemical Engineering Science 84 (2012) 218–241

Contents lists available at SciVerse ScienceDirect

Chemical Engineering Science

journal homepage: www.elsevier.com/locate/ces

A geochemical model for interpretation of chalk core flooding experiments

P.Ø. Andersen, S. Evje *, M.V. Madland, A. Hiorth

University of Stavanger (UoS), 4036 Stavanger, Norway

HIGHLIGHTS

- A transport-reaction model is developed for predicting ion concentrations in chalk core experiments.
- Experiments have been used to fit and verify parameters of the included water–rock chemistry.
- Transient and steady state concentrations are captured by the model.
- Model is relevant for enhanced oil recovery and brine-dependent deformation of chalk.

ARTICLE INFO

Article history:
Received 21 December 2011
Received in revised form
22 August 2012
Accepted 22 August 2012
Available online 31 August 2012

Keywords:
Water–rock interaction
Porous media flow
Reactive transport model
Convection–diffusion–reaction equations
Core plug experiments
Two-phase flow

ABSTRACT

We develop a model that takes into account the combined effect of transport and chemical reactions for the study of various flooding experiments with chalk cores where the flooding involves seawater-like brines. The chemical system we consider is based on a selection of the most prominent ions and minerals relevant for the lab experiments in question. We include mechanisms such as advection, diffusion, and water–rock chemistry in terms of precipitation and dissolution, ion exchange, aqueous equilibrium of carbon species, complexes, and charge balance. The aqueous chemistry and the ion exchange processes are assumed to take place instantaneously whereas kinetic is included for the dissolution/precipitation processes. An important motivation behind the development of the model is to bring forth a model that can support the study of water-weakening effects as well as brine-dependent oil recovery in the context of chalk reservoirs.

In particular, we test the performance of the proposed model by comparing with some recent flooding experiments involving $MgCl_2$ type of brines and seawater-like brines. The measured effluent concentrations reflect that there typically are some rapid transient effects for small times followed by some slower transients, and finally, convergence to steady state concentrations. For a fixed set of reaction rate constants, various standard thermodynamic constants, flow injection rate, and diffusion coefficient, the proposed model is able to capture main trends of the measured outlet ion concentrations for a set of tests with the above mentioned brines. Consequently, the model shows that the experimental behavior can possibly be understood as a result of an interplay between advection and diffusion, and water–rock interaction in terms of precipitation/dissolution of minerals and ion exchange processes. We use the model to detect the role played by the different components, in particular, the role played by the ion exchange and the dissolution/precipitation which seems important for further investigations of brine-dependent water weakening and oil-recovery mechanisms.

1. Introduction

Transport and chemical reactions have been extensively studied in the recent years. The flow of aqueous-reacting solutes through soil or porous rock involves a complex system of geochemical, hydrological, and biochemical processes and is of fundamental importance in many different contexts. The focus of this paper is on development of a simplified geochemical model that in the future can be used for studying water–rock chemistry relevant for weakening of chalk reservoirs as well as mechanisms for increased oil recovery. In the following we describe some laboratory results that can illustrate these two brine-dependent phenomena. This will serve as a motivation for the model we shall formulate in this work.

1.1. Brine-dependent stress–strain behavior and brine-dependent oil recovery

The effect of aqueous chemistry on the mechanical strength of chalk has been studied extensively from an experimental point of

* Corresponding author. Tel.: +47 51 83 17 41.
E-mail addresses: pal.andersen@uis.no (P.Ø. Andersen), steinar.evje@uis.no (S. Evje), merete.madland@uis.no (M.V. Madland), aksel.hiorth@uis.no (A. Hiorth).

0009-2509/$ - see front matter © 2012 Elsevier Ltd. All rights reserved.
http://dx.doi.org/10.1016/j.ces.2012.08.038

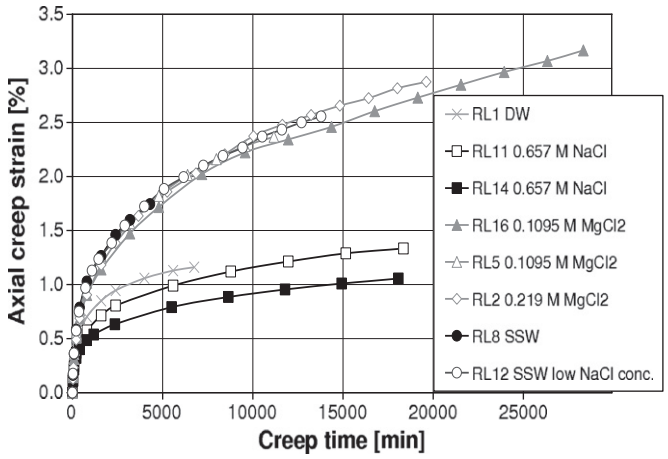

Fig. 1. An example of brine-dependent chalk weakening effect taken from Madland et al. (2011). The figure shows axial creep strain vs. creep time for Liège cores flooded with fluids with different brine compositions at 10.5 MPa differential creep stress and 130 °C. Clearly, the creep behavior is sensitive to the brine composition.

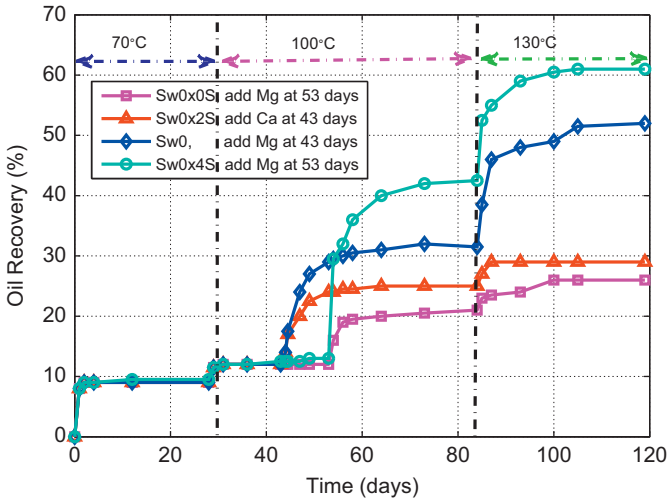

Fig. 2. Oil recovery curves for imbibition tests on chalk cores where different seawater (Sw) like brines give different oil recovery curves. In these experiments the concentration of Mg^{2+}, Ca^{2+}, and SO_4^{2-} are systematically varied. Plots have been reproduced from the work (Zhang et al., 2007) by the accuracy of an eye and must be considered as approximate.

view. It is observed that at high temperatures, like 130 °C, chalk exposed to seawater is significantly weaker than chalk exposed to distilled water (Heggheim et al., 2005; Madland et al., 2006; Korsnes et al., 2008). More recently a set of flooding experiments with NaCl, $MgCl_2$, as well as various seawater-like brines, were performed for chalk cores from Liège and Stevns Klint (Madland et al., 2011). This study clearly reflected brine-dependent stress–strain behavior. We refer to Fig. 1 for an illustration of this phenomenon. The shape of the different creep strain curves is strongly linked to the composition of the brine used for the flooding.

Another activity, but related one, is the study of how oil recovery from core plugs is sensitive to the brine composition. Many experimental studies of spontaneous imbibition for chalk core plugs have shown that seawater may change the wettability in the direction of more water-wet conditions in chalk reservoirs (Standnes and Austad, 2000, 2003; Strand et al., 2000, 2006; Zhang and Austad, 2006; Austad and Standnes, 2003; Zhang et al., 2007) and thereby give rise to a higher oil recovery. An example of this phenomenon is shown in Fig. 2.

Most likely, the explanation of these experimental results must be of a chemical nature. More precisely, the experimental studies dealing with water-induced compaction and wettability alteration in chalks, indicate rather clearly that three ions are of particular importance; Mg^{2+}, Ca^{2+} and SO_4^{2-} (Austad and Standnes, 2003; Zhang and Austad, 2006; Hiorth et al., 2010). A natural approach is then to try to identify various water–rock chemistry effects that occur when a brine with a certain composition enters the core which contains another brine that is in equilibrium with the rock inside the core. In particular, this will result in a non-equilibrium state in the pore space which will trigger chemical reactions in the aqueous phase as well as possible water–rock interaction in terms of dissolution/precipitation of minerals and/or changes in ion concentrations on the rock due to ion exchange processes.

For example, in Madland et al. (2011), in order to shed more light on the possible role played by the water–rock chemistry for these lab experiments, effluent concentrations were analyzed. A typical example is shown in Fig. 3. This shows the effluent concentrations for a flooding experiment with a $MgCl_2$ brine where the core initially is saturated with distilled water. The most striking aspect of this plot is that it reveals a significant gain of calcium ions and corresponding loss of magnesium ions. Regarding the concentration of calcium it is seen that there is a rapid increase during the first 1000 min, followed by a slower decrease over the next 7000–9000 min before a steady state effluent

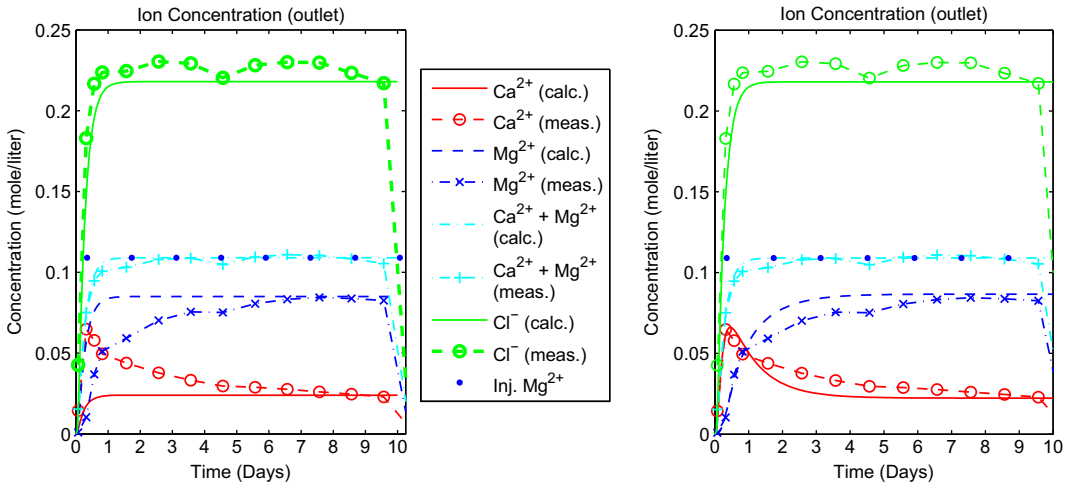

Fig. 3. Flooding with a 0.109 M $MgCl_2$ brine. Measured and calculated effluent concentrations. Left: Results similar to those produced in Evje et al. (2009) and Madland et al. (2011) where the model only takes into account dissolution/precipitation. Right: Results produced by the model developed in this paper which takes into account the combined effect of dissolution/precipitation and ion exchange processes.

concentration is reached after approximately 10 000 min. The interpretation of this behavior suggested in Madland et al. (2011) was that the transient behavior could be linked to ion exchange processes where calcium ions, initially attached to the rock surface, are released with a corresponding adsorption of magnesium ions. However, the steady gain of calcium ions and corresponding loss of magnesium ions observed at the final time of the flooding experiment, reflect that there is an ongoing dissolution of calcite and precipitation of a magnesite bearing mineral. This interpretation was supported by corresponding scanning electron microscopy (SEM) analysis showing changes in the mineral composition after flooding. More precisely, SEM images of cores after flooding with $MgCl_2$, indicated precipitation of a magnesium bearing mineral whereas flooding with seawater-like brines indicated precipitation of a sulphate bearing mineral. We refer to Madland et al. (2011) for details.

Hence, a main finding from Madland et al. (2011) was that water–rock chemistry in terms of a combined effect of dissolution/precipitation and ion exchange processes, seem to play a role in the brine-dependent stress–strain behavior. Similarly, flooding experiments carried out prior to various spontaneous imbibition experiments also seem to indicate that such processes take place and therefore potentially play a role in the observed brine-dependent oil recovery. For example in Zhang et al. (2007), measured effluent concentrations when flooding with seawater-like brines at a temperature of 130 °C, reflect desorption of calcium ions and adsorption of magnesium ions.

1.2. Purpose of this work

In (Evje et al., 2009; Madland et al., 2011) a first version of a mathematical model was developed as a help to interpret the experimental results. This model was based on a selection of the most prominent ions and minerals involved in the chemical system represented by the flooding experiments. This model incorporates aqueous chemistry, water–rock interaction in terms of mineral precipitation/dissolution, and advection and diffusion. The model was tested for flooding with $MgCl_2$. In Fig. 3 (left figure) results produced by the model are shown. It was observed that the model could explain the steady state effluent concentrations as a result of the combined effect of transport and dissolution/precipitation. However, the model did not capture the rapid transients in the initial stage of the flooding as well as the slower transients before steady state concentrations were reached.

The objective of this work is to continue the development of the water–rock chemistry model such that it contains enough details to make it relevant for the study of water-weakening effects and brine-dependent oil recovery, as described above. Note, however, that the coupling itself between the proposed water–rock chemistry model and such oil recovery mechanisms is not discussed here. In particular, the following extensions are made:

- We include some aqueous complexes potentially important for flooding with seawater-like brines. The selection is based on equilibrium calculations using the geochemical simulator PHREEQC (Parkhurst and Appelo, 1999).
- We include relevant ion exchange effects involving Ca^{2+}, Mg^{2+}, and Na^{+} ions.
- We take into account that CO_2 is dissolved in water.

The resulting, highly nonlinear and coupled system of advection–diffusion–reaction equations is solved by using an operator splitting approach. It is demonstrated that the model can capture the rapid and slow transient effects for flooding with $MgCl_2$ brines observed in the experiments, see Fig. 3 (right figure) for a result produced by the extended model. We use the model and identify more systematically the impact on the solution, respectively, from dissolution/precipitation and ion exchange. Further evaluation of the model is carried out by comparing with various flooding experiments from Madland et al. (2011) where seawater-type of brines are used. The rather complicated interplay between Ca^{2+}, Mg^{2+}, and SO_4^{2-} ions is investigated and highlighted.

1.3. Development of various geochemical simulation tools

Within the geochemical community many advanced simulators have been developed through the last decades that include combined transport-reaction effects in addition to different fluid dynamic, thermodynamic and geochemical mechanisms. Here we mention TOUGHREACT, PHAST and PHREEQC as representative examples. In the literature many interesting applications of such simulators can be found (Oelkers and Schott, 1996; Lasaga, 1998; Oelkers et al., 2009; Appelo and Postma, 2009). We also refer to seminal works like Rubin (1983) and Willis and Rubin (1987) and to Engesgaard and Kipp (1992) for a nice overview of various models and important concepts in the development of such models.

On the other hand there is a large number of more theoretical studies that have been conducted on simplified models where focus is on extracting insight into fundamental mechanisms relevant for coupled transport-reaction flows rather than very detailed simulations. For instance, it is often of interest to extract information about the long-time behavior for a reactive flow system. Examples of works in this direction are given in the following list of works (van Duijn and Knabner, 1992a,b; Knabner et al., 1995; van Duijn et al., 1998; Hilhorst et al., 1996, 2000; Bouillard et al., 2007, 2009; Aregba-Driollet et al., 2004; Ali et al., 2007a,b; Pawell and Krannich, 1996). The analytic studies of simplified models therefore possibly can bring forth insight that is not so easy to extract just by running a more complete geochemical simulator.

From our point of view, it may not be straightforward to use existing geochemical simulators as mentioned above in the context of brine-dependent chalk weakening studies where we seek to take into account stress–strain behavior or brine-dependent oil recovery studies where chemistry effects water–oil transport mechanisms. This has motivated us to formulate a transport-reaction model that is directed more precisely toward the applications we have in mind. We strive to keep the model on a relatively simple and transparent level to identify the role played by some important parameters.

We end this section by describing the structure of the remaining part of the paper. In Sections 2 and 3 we briefly review the central parts of the model as developed in Evje et al. (2009) and also explain how the new components (like aqueous complexes ion and ion exchange) have been taken into account. Then, in Section 4 we present a detailed comparison of experimental results and corresponding computed solutions. Some concluding remarks are given in Section 5.

2. The model

We now turn to the water–rock system we are going to work within the rest of this paper. The system is obtained by making an appropriate selection of important minerals and species relevant for the specific problem in question. Our choice of minerals is based on experimental observations and running equilibrium calculations by using the simulator PHREEQC as a guideline. Key observations relevant for the brines used for flooding experiments discussed in Madland et al. (2011) are:

- Calcite is the dominant mineral in chalk.
- Core flooding experiments at high temperature (130 °C) show from effluent measurements that seawater deposits magnesium

and sulfate, while $MgCl_2$ deposits magnesium (Madland et al., 2011). Calcium is produced. Subsequent SEM-EDS analysis detected the precipitation of magnesium carbonate minerals with huntite and magnesite as the most likely candidates, but also magnesium–silicon minerals formed from dissolved silicates initially present in the chalk. Flooding seawater (with low NaCl content) also produced the sulfate mineral anhydrite.

- Seawater at 130 °C temperature was considered in PHREEQC. It is oversaturated on several magnesium-based minerals such as artinite, brucite, dolomite, huntite and magnesite. At equilibrium with calcite there is still oversaturation of dolomite, huntite and magnesite, but not artinite and brucite.
- For a 0.219 M $MgCl_2$ brine at the same temperature all the stated magnesium-based minerals are undersaturated, however, when at equilibrium with calcite they are all oversaturated.
- Due to the uncertainty regarding the magnesium-based minerals and the fact that a lot of them have similar behavior in terms of saturation index, we select one of them, magnesite, as a representative to all of them. This choice is supported by the SEM–EDS observations. In reality, there might be several magnesium-minerals involved.
- For the seawater there are no oversaturated sulfate-based minerals at 130 °C, not even when the brine is in equilibrium with calcite. However, if there is equilibrium with both calcite and magnesite the mineral anhydrite is oversaturated. It is selected as the sulfate-based mineral.

Summarized we include the minerals calcite, magnesite and anhydrite in our model, but point out that this selection can be expanded. Relevant inclusions for future investigations could be huntite, brucite and silicates.

The choice of cations interacting with the surface is based on the following observations:

- Concentration peaks or delays in the effluent of flooding experiments reveal that there is an adsorption/desorption process occurring (Madland et al., 2011).
- It has been documented that Ca^{2+}, Mg^{2+} and SO_4^{2-} are potential determining ions towards the chalk surface (Strand et al., 2006; Zhang et al., 2007). SO_4^{2-} adsorption has been demonstrated in (Strand et al., 2007) at surface temperatures.
- The experimental observations seem to indicate that Na^+ to some extent is able to exchange with other cations. This could be due to clay minerals in the chalk since Na^+ is not known to be attracted to the calcite surface. However, the formulation that is employed does not rule out that the relatively high concentration of Na^+ allows this ion to displace some of the cations also on the calcite surface.

Hence, the surface species taken into account and discussed in the current version of the model are Ca^{2+}, Mg^{2+} and Na^+. Adsorption of SO_4^{2-} is left for future investigations.

Based on these observations we then define the chemical system as composed of the following set of ions and minerals, accompanied by their respective variables:

$\rho_c = [CaCO_3]$ (solid)	$C_{ca} = [Ca^{2+}]$ (aq)	$C_h = [H^+]$ (aq)
$\rho_g = [CaSO_4]$ (solid)	$C_{mg} = [Mg^{2+}]$ (aq)	$C_{oh} = [OH^-]$ (aq)
$\rho_m = [MgCO_3]$ (solid)	$C_{so} = [SO_4^{2-}]$ (aq)	$C_{hco} = [HCO_3^-]$ (aq)
	$C_{Na} = [Na^+]$ (aq)	$C_{co} = [CO_3^{2-}]$ (aq)
	$C_{Cl} = [Cl^-]$ (aq)	$C_{co2} = [CO_2]$ (aq)
$\rho^s_{Na} = [na^+]$ (surface)	$\rho^s_{ca} = [Ca^{2+}]$ (surface)	$\rho^s_{mg} = [Mg^{2+}]$ (surface)

The primary unknowns are the concentrations of minerals represented by ρ (mol per liter rock): ρ_c, ρ_g, ρ_m; concentrations of species represented by C (mol per liter of solution): C_{ca}, C_{so}, C_{mg}, C_{na}, C_{cl}, C_h, C_{oh}, C_{co}, C_{hco} and C_{co2}; and concentrations of cation species on the surface in terms of ρ (mol per liter rock): ρ^s_{na}, ρ^s_{ca} and ρ^s_{mg}. Hence, the concentration C of a species expressed in terms of mol per liter rock is given by ϕC where ϕ is porosity. Note that by a volume rock we include the grains and the porous space.

In the model we include chemical kinetics associated with the concentrations ρ_c, ρ_g, ρ_m, C_{ca}, C_{so}, C_{mg} involved in the water–rock interactions (dissolution/precipitation), whereas the concentrations C_h, C_{oh}, C_{co}, C_{hco} and C_{co2} involved in the aqueous chemistry and the surface concentrations ρ^s_{na}, ρ^s_{ca} and ρ^s_{mg}, are obtained by considering equilibrium state equations and charge balance.

2.1. Chemical reactions

The chemical reactions for water–rock interaction (dissolution/precipitation) we include in the transient model are:

$$CaCO_3(s) \rightleftharpoons Ca^{2+} + HCO_3^- - H^+,$$

$$CaSO_4(s) \rightleftharpoons Ca^{2+} + SO_4^{2-},$$

$$MgCO_3(s) \rightleftharpoons Mg^{2+} + HCO_3^- - H^+. \quad (1)$$

In addition to (1), we take into consideration the following chemical reactions for the aqueous chemistry which describe the carbon chemistry and water dissociation:

$$CO_2(g) + H_2O \rightleftharpoons HCO_3^- + H^+,$$

$$CO_2(aq) + H_2O \rightleftharpoons HCO_3^- + H^+,$$

$$HCO_3^- \rightleftharpoons CO_3^{2-} + H^+,$$

$$H_2O \rightleftharpoons OH^- + H^+. \quad (2)$$

We also include some potentially important aqueous complexes for the system in question. This is relevant, in particular, for flooding with seawater-like brines at high temperature. The selection of these ions is based on equilibrium calculations using PHREEQC.

$$CaSO_4^0 \rightleftharpoons Ca^{2+} + SO_4^{2-},$$

$$NaSO_4^- \rightleftharpoons Na^+ + SO_4^{2-},$$

$$MgSO_4^0 \rightleftharpoons Mg^{2+} + SO_4^{2-}$$

$$CaCl^+ \rightleftharpoons Ca^{2+} + Cl^-$$

$$MgCl^+ \rightleftharpoons Mg^{2+} + Cl^-. \quad (3)$$

Finally, we also take into account that equilibrium reactions between the rock surface and liquid for the modeling of ion exchange processes relevant for the laboratory results presented in Madland et al. (2011). We follow the exchange reaction formulation given in Appelo and Postma (2009) and assume that Ca^{2+}, Mg^{2+} and Na^+ can all participate in the exchange reactions as expressed by the following reactions:

$$Na^+ + 1/2CaX_2 \rightleftharpoons NaX + 1/2Ca^{2+},$$

$$Na^+ + 1/2MgX_2 \rightleftharpoons NaX + 1/2Mg^{2+}, \quad (4)$$

where the X^- is to be interpreted as a free site on the surface. Note that the ion exchange formulation is at this stage based on that of clays as formulated in Appelo and Postma (2009) to incorporate the main mechanism and to keep the description at a simple level consistent with rest of the model formulation. Finer details concerning the surface chemistry of calcite should be included in a later version of the model to make it more

realistic and improve its predictive force. In particular, a more comprehensive and professional description of the chalk surface chemistry, instead of the use of (4), could be made by considering theory of diffuse double layer, surface charge and zeta potential. As calcite is different from clays the equilibrium constants for the chemical reactions are uncertain. However, the experiments can detect which cations that have a potential for adsorption. Na^+ will probably not adsorb on calcite, but to clay elements in the chalk matrix.

It is implicitly assumed that the reactions (2), (3), and (4) take place at a much shorter time scale than the dissolution/precipitation processes (1). In the remaining part of this section, we first give some more details concerning the equilibrium chemistry associated with the chemical reactions (2), (3), and (4). Then, we describe the relations that take into account kinetics associated with the precipitation/dissolution processes (1). Finally, in Section 3 the combined effect of these chemical reactions and transport of ions are taken into account.

2.2. Preliminaries

We use the following notation for the *total fluid concentration* of the basis species Ca^{2+}, Mg^{2+}, SO_4^{2-}, Na^+, Cl^-, and TIC (total inorganic carbon):

$$C_{ca} = m_{ca} + n_{caso} + n_{cacl},$$

$$C_{mg} = m_{mg} + n_{mgso} + n_{mgcl},$$

$$C_{so} = m_{so} + n_{caso} + n_{naso} + n_{mgso},$$

$$C_{na} = m_{na} + n_{naso},$$

$$C_{cl} = m_{cl} + n_{mgcl} + n_{cacl},$$

$$C_{TIC} = m_{hco} + m_{co} + m_{co2}. \tag{5}$$

Here m is used to represent concentration of basis species whereas n is used to represent concentration of aqueous complexes. A main assumption is that the total concentration C of a species changes by different mechanisms of mass transfer while being distributed into its different subspecies m, n locally by equilibrium.

We shall distinguish between concentration m, n and chemical activity a noting that they are related by Lasaga (1998) and Appelo and Postma (2009)

$$a = \gamma m, \tag{6}$$

and similarly for n, where γ is the activity coefficient. Note that molality and not molarity should be used in (6) for m. However, we assume the difference is negligible by implicitly assuming 1 l brine corresponds to 1 kg water.

According to the Truesdell and Jones equation (Appelo and Postma, 2009) the activity coefficient γ_i is given by

$$\log_{10}(\gamma_i) = -\frac{A(T)Z_i^2\sqrt{I_0}}{1 + a_i B(T)\sqrt{I_0}} + b_i I_0, \tag{7}$$

where the index i refers to the different species involved in the system which is studied. Moreover, Z_i refers to the ionic charges, $A(T)$ and $B(T)$ are temperature dependent given functions (Helgeson et al., 1981; Hiorth et al., 2008). a_i,b_i are ion specific constants (Appelo and Postma, 2009), whereas I_0 refers to the ionic strength defined by

$$I_0 = \frac{1}{2}\left(\sum_i^{N_b} m_i Z_i^2 + \sum_i^{N_c} n_i Z_i^2\right). \tag{8}$$

For the numerical calculations of Section 4, we calculate I_0 based on the equilibrium ion concentrations for the injected brine. Consequently, I_0 is assumed to be constant throughout the flooding. Since the temperature is kept constant, the activity coefficients are also taken to be constant, according to (7). A rough estimate of the I_0 is given by

$$I_0 = \frac{1}{2}\sum_i^{N_b} C_i Z_i^2. \tag{9}$$

Note that the inclusion of complexes has the effect of reducing the total concentration of moles and of charge. As a result the effective ionic strength (8) is reduced compared to assuming a fully dissociated solution (9). In the experiments we use brines having ionic strength similar to seawater (I_0=0.7) and require that the calculation of activity coefficients is made with formulas applicable in that range. Truesdell Jones formula meets this requirement and is used for the charged uncomplexed species. The complexed species had less available parameter data and required the use of other formulas.

The Davies equation is another relation often used to calculate activity coefficients and is applicable up to an ionic strength of about 0.5.

$$\log_{10}(\gamma_i) = -\frac{A(T)Z_i^2\sqrt{I_0}}{1+\sqrt{I_0}} + 0.3A(T)Z_i^2 I_0, \tag{10}$$

where $A(T)$ is the same temperature dependent coefficient as in (7). Note that it is similar to Truesdell Jones formula, but treats ions with equal valence the same. It is used for the activity coefficients of the charged complexes.

Finally the activity coefficients for uncharged species are given by Setchenows formula (which follows from Truesdell Jones)

$$\log_{10}(\gamma_i) = b_i I_0, \tag{11}$$

assuming b_i=0.1. Numerical values of a_i,b_i,$A(T)$,$B(T)$ used for the simulations in Section 4 are provided in Appendix C.2.

2.3. Aqueous chemistry

The local equilibrium associated with the reactions in (2) gives the following relations:

$$K = \frac{a_{hco}a_h}{P_{co2}} = \frac{(\gamma_{hco}\gamma_h)m_{hco}m_h}{P_{co2}}, \tag{12}$$

$$K_{co2} = \frac{a_{hco}a_h}{a_{co2}} = \frac{\gamma_{hco}\gamma_h}{\gamma_{co2}}\frac{m_{hco}m_h}{m_{co2}}, \tag{13}$$

$$K_{hco} = \frac{a_{co}a_h}{a_{hco}} = \left(\frac{\gamma_{co}\gamma_h}{\gamma_{hco}}\right)\frac{m_{co}m_h}{m_{hco}}, \tag{14}$$

$$K_w = a_h a_{oh} = (\gamma_{oh}\gamma_h)m_{oh}m_h, \tag{15}$$

where the constants K, K_{co2}, K_{hco} and K_w are known equilibrium constants.

When mixing a brine at atmospheric conditions it is often a good assumption to use the atmospheric partial pressure of CO_2

$$P_{co2} = P_{co2}^{atm} = 10^{-3.5} \quad \text{(bar)}. \tag{16}$$

A known and constant P_{co2} is reasonable for a brine in equilibrium with a gas of constant composition. However, when the system is closed, pressurized and heated to obtain reservoir-like conditions (p^{res},T^{res}), the equilibrium constants and activity coefficients will change (as long as the fluid is not boiling the pressure dependence here is negligible). The equilibrium of the system will shift so we need to calculate the P_{co2}^{res} to be used at T^{res}, as this property is temperature-dependent.

First we consider the atmospheric conditions: We determine the equilibrium state of the given brine by solving Eqs. (5), (7), (8), (10)–(16), combined with the charge balance Eq. (32) defined in Section 2.5. From the output of these calculations we determine

the concentration of dissolved carbon at atmospheric conditions represented by $C_{TIC}(T^{atm})$, as given by the last equation of (5)

$$C_{TIC} = m_{hco} + m_{co} + m_{co2}, \tag{17}$$

This property is conserved at the new temperature before injection

$$C_{TIC}(T^{res}) = C_{TIC}(T^{atm}). \tag{18}$$

In other words, at the new temperature T^{res} the P^{res}_{co2} becomes unknown in (12) whereas we require that (17) and (18) hold.

At T^{res} we make a full equilibrium calculation of the brine by solving Eqs. (5), (7), (8), (10)–(15), (17), (18), and (32) to find the individual concentrations. The P^{res}_{co2} then follows from (12).

To conclude, we will assume that the P^{res}_{co2} is constant during a flooding experiment, but let it be determined by the injected brine and the temperature as described above. This assumption leads to a constant concentration of aqueous CO_2 as can be seen by combining Eqs. (12) and (13):

$$a_{co2} = \frac{P_{co2}K}{K_{co2}}. \tag{19}$$

We then absorb the constant partial pressure into a new constant by defining

$$K_{co} \equiv P_{co2}K. \tag{20}$$

Remark 1. We performed equilibrium calculations (using PHREEQC) for the brines discussed in Section 4 (SSW-I and $MgCl_2$-I) showing that going from 25 °C to 130 °C the $\log(P_{co2})$ changed from −3.5 to −2.9 and −2.0, respectively. To see whether it was reasonable to keep this new value constant during a flooding experiment we let the system reach equilibrium with dissolution of calcite and precipitation of magnesite and anhydrite. The $\log(P_{co2})$ for SSW-I then changed from −2.0 to −1.2, while that of $MgCl_2$-I changed from −2.9 to −3.4. Apparently the change with temperature was the most important, also because the brines do not actually reach equilibrium with the mineral phases during the flooding experiments. This justifies as a reasonable approximation to keep the P_{co2} constant but dependent on brine and temperature as outlined above.

2.3.1. Aqueous complexes

The formation of aqueous complexes can be described by equilibria of the reactions (3). Applying the law of mass action we get the following algebraic equations:

$$K_{caso} = \frac{a_{ca}a_{so}}{a_{caso}} = (\gamma_{ca}\gamma_{so})\frac{m_{ca}m_{so}}{n_{caso}},$$

$$K_{naso} = \frac{a_{na}a_{so}}{a_{naso}} = (\gamma_{na}\gamma_{so})\frac{m_{na}m_{so}}{n_{naso}},$$

$$K_{mgso} = \frac{a_{mg}a_{so}}{a_{mgso}} = (\gamma_{mg}\gamma_{so})\frac{m_{mg}m_{so}}{n_{mgso}},$$

$$K_{cacl} = \frac{a_{ca}a_{cl}}{a_{cacl}} = (\gamma_{ca}\gamma_{cl})\frac{m_{ca}m_{cl}}{n_{cacl}},$$

$$K_{mgcl} = \frac{a_{mg}a_{cl}}{a_{mgcl}} = (\gamma_{mg}\gamma_{cl})\frac{m_{mg}m_{cl}}{n_{mgcl}}, \tag{21}$$

where K_i refers to the equilibrium constant (or dissociation constant which is the inverse of K_i) (Appelo and Postma, 2009) for the aqueous complex i. Note that in combination with (5) we then get the following expressions for the total concentrations:

$$C_{ca} = m_{ca} + \tilde{K}^{-1}_{caso} m_{ca}m_{so} + \tilde{K}^{-1}_{cacl} m_{ca}m_{cl},$$

$$C_{mg} = m_{mg} + \tilde{K}^{-1}_{mgso} m_{mg}m_{so} + \tilde{K}^{-1}_{mgcl} m_{mg}m_{cl},$$

$$C_{so} = m_{so} + \tilde{K}^{-1}_{caso} m_{ca}m_{so} + \tilde{K}^{-1}_{mgso} m_{mg}m_{so} + \tilde{K}^{-1}_{naso} m_{na}m_{so},$$

$$C_{na} = m_{na} + \tilde{K}^{-1}_{naso} m_{na}m_{so},$$

$$C_{cl} = m_{cl} + \tilde{K}^{-1}_{cacl} m_{ca}m_{cl} + \tilde{K}^{-1}_{mgcl} m_{mg}m_{cl}, \tag{22}$$

where we use the notation

$$\tilde{K}_{caso} = \frac{K_{caso}}{\gamma_{ca}\gamma_{so}}, \quad \tilde{K}_{mgso} = \frac{K_{mgso}}{\gamma_{mg}\gamma_{so}}, \quad \tilde{K}_{naso} = \frac{K_{naso}}{\gamma_{na}\gamma_{so}},$$

$$\tilde{K}_{cacl} = \frac{K_{cacl}}{\gamma_{ca}\gamma_{cl}}, \quad \tilde{K}_{mgcl} = \frac{K_{mgcl}}{\gamma_{mg}\gamma_{cl}}. \tag{23}$$

From this we find that

$$m_{ca} = \frac{C_{ca}}{1 + m_{so}\tilde{K}^{-1}_{caso} + m_{cl}\tilde{K}^{-1}_{cacl}},$$

$$m_{mg} = \frac{C_{mg}}{1 + m_{so}\tilde{K}^{-1}_{mgso} + m_{cl}\tilde{K}^{-1}_{mgcl}},$$

$$m_{na} = \frac{C_{na}}{1 + m_{so}\tilde{K}^{-1}_{naso}},$$

$$m_{so} = C_{so} \Bigg/ \left(1 + \frac{C_{mg}}{\left(\tilde{K}_{mgso} + m_{so} + m_{cl}\frac{\tilde{K}_{mgso}}{\tilde{K}_{mgcl}}\right)} + \frac{C_{ca}}{\left(\tilde{K}_{caso} + m_{so} + m_{cl}\frac{\tilde{K}_{caso}}{\tilde{K}_{cacl}}\right)} + \frac{C_{na}}{(\tilde{K}_{naso} + m_{so})} \right),$$

$$m_{cl} = C_{cl} \Bigg/ \left(1 + \frac{C_{mg}}{\tilde{K}_{mgcl} + m_{so}\frac{\tilde{K}_{mgcl}}{\tilde{K}_{mgso}} + m_{cl}} + \frac{C_{ca}}{\tilde{K}_{cacl} + m_{so}\frac{\tilde{K}_{cacl}}{\tilde{K}_{caso}} + m_{cl}} \right). \tag{24}$$

Implicitly we find $(m_{so}, m_{cl}) = f(C_{ca}, C_{mg}, C_{so}, C_{na}, C_{cl})$ from the two last equations of (24). This is done by considering an initial guess $(m_{so}, m_{cl})^0 = (0,0)$ and use the above two expressions to update the estimates until convergence is attained. Then we can calculate m_{ca}, m_{mg}, and m_{na} straightforwardly from the three first equations of (24). Hence, we have a mapping

$$(C_{ca}, C_{mg}, C_{so}, C_{na}, C_{cl}) \rightarrow (m_{ca}, m_{mg}, m_{so}, m_{na}, m_{cl}), \tag{25}$$

between the total concentrations C_i and the basis species m_i.

The complexes are taken into account in the full transient model in an approximate manner by using the following approximation: We assume that the fraction r_i of free (uncomplexed) ions relative to the total concentration of the species, is a constant for each ion and that this fraction depends only on the injected brine:

$$r_i := \frac{m_i}{C_i}, \quad (i = na, cl, ca, so, mg). \tag{26}$$

The advantage of this assumption is that we can reduce the nonlinear coupling of the system of equations by replacing all m_i with $r_i C_i$ in the equilibrium and rate expressions, see Sections 2.4 and 2.6.

Table 1
Selected simulations in PHREEQC of fractions r_i of free ions compared to total species in solution at 130 °C. We refer to Appendix C.4 for the brine compositions. Here r_i was calculated in a *Free* solution and a solution in *Equilibrium* with a system where calcite can dissolve and magnesite and anhydrite can precipitate.

Brine	$MgCl_2$	(0.219 M)	SSW-I		Na_2SO_4	(0.219 M)
State	Free	Equilibrium	Free	Equilibrium	Free	Equilibrium
r_{ca}	0.95[a]	0.95	0.88	0.91	0.35[a]	0.34
r_{so}	0.03[a]	0.09[a]	0.19	0.32	0.77	0.77
r_{mg}	0.82	0.81	0.47	0.57	0.03[a]	0.03[a]
r_{na}	0.94[a]	0.94[a]	0.92	0.93	0.88	0.88
r_{cl}	0.91	0.95	0.93	0.93	0.94[a]	0.94[a]

[a] In these cases the given species was not in the original system and 0.001 M of its salt with Na^+ or Cl^- was added.

The fraction to be used, and calculated by employing the mapping (25) described above, will be an average of the free solution (representative of inlet conditions) and the solution in equilibrium with a system where calcite can dissolve and magnesite and anhydrite can precipitate (representative of outlet conditions). Both estimates are taken at the same temperature. To validate the use of the mapping (25) we made simulations in PHREEQC, summarized in Table 1. In particular, we observed that the values for r_i produced by the simplified model was in the same range as the results shown in Table 1. Solutions of $MgCl_2$, seawater SSW-I and Na_2SO_4 (compositions are found in Appendix C.4) at 25 °C in equilibrium with atmosphere ($P_{co2}^{atm} = 10^{-3.5}$) have been considered at 130 °C and the fractions of free ions calculated.

The results show that for some brines a lot of the species are bound in complexes, especially for sulphate and magnesium. Therefore it can be highly relevant to include these complexes. Also, note that although the fraction r_i changes with species and brine it does not change much from the free state to the equilibrium state. Consequently, this justifies the assumption to use a constant fraction r_i. Complexes that generally tie up more than 5% of the species for different brines were selected in this paper.

2.4. Ion exchange

Ion exchange is the phenomenon that a charged surface stores a given amount of charge to be in local electrical charge balance. The ions attached to the surface are in equilibrium with the surrounding brine. Therefore a change in the brine composition will typically induce a combination of adsorption of ions from brine and desorption of ions from surface. We will assume that the chalk surface has a constant capacity and that the cations Ca^{2+}, Mg^{2+}, and Na^+ occupy the exchanger.

The cation exchange capacity is defined as the capacity of *equivalents* (valence times molar concentration) per unit rock and is commonly measured in *meq* per kg bulk rock (Appelo and Postma, 2009; Langmuir, 1997). It is more convenient to express this in rock concentrations (eq per liter rock) by the conversion

$$CEC[\text{eq/l rock}] = 1000 \cdot CEC\ [\text{meq/kg solid}] \cdot \omega_c[\text{kg solid/l solid}](1-\phi). \quad (27)$$

It is assumed that the *CEC* is constant. The initial surface rock concentration for each cation is specified, $(\rho_{ca}^{s,0},\rho_{mg}^{s,0},\rho_{na}^{s,0})$ [mol/l], and the CEC [eq/l] is defined as:

$$CEC = \sum_{i:cations} Z_i\rho_i^s = 2\rho_{ca}^{s,0} + 2\rho_{mg}^{s,0} + \rho_{na}^{s,0}. \quad (28)$$

We have used the Gaines–Thomas convention for ion exchange, as in PHREEQC (Parkhurst and Appelo, 1999). This means using the fraction of equivalents as the activity for the species on the surface:

$$\beta_i = \frac{\rho_i^s Z_i}{\sum \rho_i^s Z_i} = \frac{\rho_i^s Z_i}{CEC} \quad (i = na,ca,mg). \quad (29)$$

Having in mind that we want to take into account the ion exchange processes represented by (4), we at a given time require

- the ionic strength I_0 and activity coefficients γ_i;
- the fraction of free ions r_i defined by (26);
- ion exchange equilibrium constants $K_{na/ca}$ and $K_{na/mg}$ for the reactions (4);
- the total concentration of ions ρ_i^{tot} which is composed of one component in water $\rho_{i,0}$ and one on the surface $\rho_{i,0}^s$ at a given time and position before the equilibrium calculation, $i = na, ca, mg$;
- the sum of equivalents fractions β_i to be 1;
- mole conservation given by total concentration preservation.

During the ion exchange process the total concentration ρ_i^{tot} remains constant while a redistribution of ions take place leading to updated equilibrium concentrations ρ_i and ρ_i^s. There are 12 unknowns in our system:

$$\rho_{ca}^s,\rho_{mg}^s,\rho_{na}^s,\rho_{ca},\rho_{mg},\rho_{na},\beta_{ca},\beta_{mg},\beta_{na},m_{ca},m_{mg},m_{na}. \quad (30)$$

The new variables here are $\rho_{ca}^s,\rho_{mg}^s,\rho_{na}^s$ and $\beta_{ca},\beta_{mg},\beta_{na}$ which represent ion concentrations on the rock surface, whereas $\rho_{ca},\rho_{mg},\rho_{na}$ are directly related to the total concentrations C_{ca},C_{mg},C_{na} introduced before. Based on what has been described so far, we obtain the following 12 mathematical equations that must be solved simultaneously:

$$K_{na/ca} = \frac{\beta_{na}}{\beta_{ca}^{0.5}} \frac{\gamma_{ca}^{0.5} m_{ca}^{0.5}}{\gamma_{na} m_{na}},$$

$$K_{na/mg} = \frac{\beta_{na}}{\beta_{mg}^{0.5}} \frac{\gamma_{mg}^{0.5} m_{mg}^{0.5}}{\gamma_{na} m_{na}},$$

$$\beta_{ca} + \beta_{mg} + \beta_{na} = 1,$$

$$\rho_{ca}^s + \rho_{ca} = \rho_{ca}^{tot},$$

$$\rho_{mg}^s + \rho_{mg} = \rho_{mg}^{tot},$$

$$\rho_{na}^s + \rho_{na} = \rho_{na}^{tot},$$

$$\rho_{ca}^s \cdot 2 = \beta_{ca} \cdot CEC,$$

$$\rho_{mg}^s \cdot 2 = \beta_{mg} \cdot CEC,$$

$$\rho_{na}^s \cdot 1 = \beta_{na} \cdot CEC,$$

$$m_{ca} = r_{ca}\rho_{ca}/\phi,$$

$$m_{mg} = r_{mg}\rho_{mg}/\phi,$$

$$m_{na} = r_{na}\rho_{na}/\phi. \quad (31)$$

The procedure for this is given in Appendix A.1. The main idea is that knowing the total concentrations ρ_i^{tot} and *CEC* for the rock we consider, we can calculate ρ_i,ρ_i^s,β_i from (31). The way the ion exchange processes are taken into account in the full transient model that couples transport and chemical reactions will be explained more precisely in Appendix B.

Remark 2. As the notation has been based on clay surface chemistry as described in Appelo and Postma (2009) and not chalk, the parameters (like *CEC* and *K*) may not be directly transferable but can indicate approximate values for this type of

modeling. Future work should incorporate more details specific to the nature of the chalk surface as a natural step in improving the prediction of water–rock interactions in chalk.

2.5. The electroneutrality condition

The following aqueous charge balance equation is assumed to hold for the various species contained in the water phase:

$$\sum_i^{N_b} m_i Z_i + \sum_i^{N_c} n_i Z_i = 0. \tag{32}$$

This allows to solve for m_h, m_{hco}, m_{co}, and m_{oh} given C_{ca}, C_{so},C_{mg},C_{na},C_{cl}. The details are given in Appendix A.2. Most importantly the aqueous concentrations can be written in the form

$$m_h = \frac{1}{2}\left(-M + \sqrt{M^2 + 4(\tilde{K}_{co} + \tilde{K}_w)}\right), \quad m_{hco} = \frac{\tilde{K}_{co}}{m_h}, \tag{33}$$

where $M(C_{ca},C_{so},C_{mg};C_{na},C_{cl}),\tilde{K}_{co},\tilde{K}_w$ are known and m_{co} and m_{oh} can be determined from (14) and (15).

2.6. Rate equations for the water–rock interaction

The rate equations associated with the water–rock interaction, as described by the dissolution/precipitation processes (1), are obtained by following an approach similar to that in Bouillard et al. (2007), see also references therein like (Lasaga, 1998) (chapter 1) and (Steefel and Lasaga, 1994). An excellent review is also given in Morse and Arvidson (2002). The main point of this approach is the use of an empirical rate equation of the form

$$R = k \cdot \mathrm{sgn}(1-\Omega)\left|1-\Omega\right|^n, \tag{34}$$

where R is the rate (positive for dissolution), $k>0$ and $n>0$ are empirical fitting terms and $(1-\Omega)$ the degree of disequilibrium with the mineral in question. Ω is the ratio of the ion activity product (IAP) to the solubility product K for the solid in question, that is, $\Omega = \mathrm{IAP}/K$.

Note that the relation between k and n determines how sensitive the rate will be to a deviation from equilibrium. Fitting the distributions of simulated mineral precipitation with experimental results will provide good estimates for these values, although such an undertaking is left for future work.

If $0<1-\Omega$ the solution is undersaturated which may lead to dissolution; if $0>1-\Omega$ the solution is supersaturated which implies precipitation. We have thus assumed that the rate of a reaction depends on one variable, Ω, and that precipitation and dissolution can be described by the same formula. A more detailed reaction kinetics can improve the model. We refer to Evje et al. (2009) for more motivation and more details and note that the reaction terms $\dot{r}_i$, for $i=c,g,m$ associated with (1), are given as follows:

$$\begin{aligned}
\dot{r}_c &= \pm\left|k_+^c a_c - k_-^c \frac{a_{ca}a_{hco}}{a_h}\right|^{n_c} = \pm (k_+^c)^{n_c}\left|1-\frac{a_{hco}a_{ca}}{K^c a_h}\right|^{n_c} \\
&= \pm k^c\left|1-\frac{\gamma_{ca}\gamma_{hco}m_{ca}m_{hco}}{\gamma_h m_h K^c}\right|^{n_c} \\
&= \pm k^c\left|1-\left[\frac{\gamma_{ca}K_{co}r_{ca}}{\gamma_h^2 K^c}\right]\frac{C_{ca}}{m_h^2}\right|^{n_c} = \pm k^c\left|1-\Omega_c\right|^{n_c},
\end{aligned} \tag{35}$$

$$\begin{aligned}
\dot{r}_g &= \pm\left|k_+^g a_g - k_-^g a_{ca}a_{so}\right|^{n_g} = \pm (k_+^g)^{n_g}\left|1-\frac{a_{ca}a_{so}}{K^g}\right|^{n_g} \\
&= \pm k^g\left|1-\frac{\gamma_{ca}m_{ca}\gamma_{so}m_{so}}{K^g}\right|^{n_g} \\
&= \pm k^g\left|1-\left[\frac{\gamma_{ca}\gamma_{so}r_{ca}r_{so}}{K^g}\right]C_{ca}C_{so}\right|^{n_g} = \pm k^g\left|1-\Omega_g\right|^{n_g},
\end{aligned} \tag{36}$$

$$\begin{aligned}
\dot{r}_m &= \pm\left|k_+^m a_m - k_-^m \frac{a_{mg}a_{hco}}{a_h}\right|^{n_m} = \pm (k_+^m)^{n_m}\left|1-\frac{a_{hco}a_{mg}}{K^m a_h}\right|^{n_m} \\
&= \pm k^m\left|1-\frac{\gamma_{mg}\gamma_{hco}m_{mg}m_{hco}}{\gamma_h m_h K^m}\right|^{n_m} \\
&= \pm k^m\left|1-\left[\frac{\gamma_{mg}K_{co}r_{mg}}{\gamma_h^2 K^m}\right]\frac{C_{mg}}{m_h^2}\right|^{n_m} = \pm k^m\left|1-\Omega_m\right|^{n_m},
\end{aligned} \tag{37}$$

where

$$\begin{aligned}
&K^c = \frac{k_+^c}{k_-^c}, \quad k^c = (k_+^c)^{n_c}, \quad \Omega_c = \left[\frac{\gamma_{ca}K_{co}r_{ca}}{\gamma_h^2 K^c}\right]\frac{C_{ca}}{m_h^2}, \\
&K^g = \frac{k_+^g}{k_-^g}, \quad k^g = (k_+^g)^{n_g}, \quad \Omega_g = \left[\frac{\gamma_{ca}\gamma_{so}r_{ca}r_{so}}{K^g}\right]C_{ca}C_{so}, \\
&K^m = \frac{k_+^m}{k_-^m}, \quad k^m = (k_+^m)^{n_m}, \quad \Omega_m = \left[\frac{\gamma_{mg}K_{co}r_{mg}}{\gamma_h^2 K^m}\right]\frac{C_{mg}}{m_h^2}.
\end{aligned} \tag{38}$$

Here a_j represents chemical activity associated with species j. Moreover, we have used that the ion activity of a solid component (the mineral) is set to one, see for example Bouillard et al. (2007). That is, we have set $a_c = a_g = a_m = 1$ in (35)–(37). k_-^j represents the rate of precipitation whereas k_+^j represents the rate of dissolution associated with the different species $j=c,g,m$ corresponding to $CaCO_3$, $CaSO_4$, and $MgCO_3$. Similarly, K^j is used to represent the equilibrium constant (solubility product) associated with the different minerals $j=c,g,m$. These are known values. On the other hand, much less is known about the rate of precipitation/dissolution represented by k_+^j and k_-^j. Note also that we have used (26) to obtain rate expressions in terms of total concentrations C. It is convenient to introduce the notation

$$\begin{aligned}
&F_c(C_{ca},C_{so},C_{mg};C_{na},C_{cl}) \overset{\mathrm{def}}{:=} \left(1-\left[\frac{\gamma_{ca}K_{co}r_{ca}}{\gamma_h^2 K^c}\right]\frac{C_{ca}}{m_h^2}\right), \\
&F_g(C_{ca},C_{so},C_{mg};C_{na},C_{cl}) \overset{\mathrm{def}}{:=} \left(1-\left[\frac{\gamma_{ca}\gamma_{so}r_{ca}r_{so}}{K^g}\right]C_{ca}C_{so}\right), \\
&F_m(C_{ca},C_{so},C_{mg};C_{na},C_{cl}) \overset{\mathrm{def}}{:=} \left(1-\left[\frac{\gamma_{mg}K_{co}r_{mg}}{\gamma_h^2 K^m}\right]\frac{C_{mg}}{m_h^2}\right).
\end{aligned} \tag{39}$$

Then we get the following rate equations associated with the minerals represented by ρ_c, ρ_g, and ρ_m:

$$\begin{aligned}
&\frac{d\rho_c}{dt} = -\phi\dot{r}_c = -\phi k^c(\max(0,F_c)^{n_c} - \max(0,-F_c)^{n_c}), \\
&\frac{d\rho_g}{dt} = -\phi\dot{r}_g = -\phi k^g(\max(0,F_g)^{n_g} - \max(0,-F_g)^{n_g}), \\
&\frac{d\rho_m}{dt} = -\phi\dot{r}_m = -\phi k^m(\max(0,F_m)^{n_m} - \max(0,-F_m)^{n_m}),
\end{aligned} \tag{40}$$

where the porosity ϕ appears in order to convert the rates from the porous volume to the rock volume.

An important constraint is to take into account the fact that mineral dissolution stops once the mineral has disappeared (Bouillard et al., 2007; Evje et al., 2009). To build this mechanism into the rate equations given by (35)–(37), we use (39) and change these equations in the following manner:

$$\begin{aligned}
&\dot{r}_c = k^c[\mathrm{sgn}^+(\rho_c)(F_c^+)^{n_c} - (F_c^-)^{n_c}], \\
&\dot{r}_g = k^g[\mathrm{sgn}^+(\rho_g)(F_g^+)^{n_g} - (F_g^-)^{n_g}], \\
&\dot{r}_m = k^m[\mathrm{sgn}^+(\rho_m)(F_m^+)^{n_m} - (F_m^-)^{n_m}],
\end{aligned} \tag{41}$$

where

$$\mathrm{sgn}^+(x)=\begin{cases}1, & \text{if } x\geq 0;\\ 0, & \text{otherwise,}\end{cases}$$

$$F_I=F_I^+-F_I^-,\quad \text{where}\quad F_I^+=\max(0,F_I),\quad F_I^-=\max(0,-F_I)$$

and $F_I^{\pm}=F_I^{\pm}(C_{ca},C_{so},C_{mg};C_{na},C_{cl})$. Clearly, in view of (40), we see that for $F_I<0$ where $I=c, g, m$ represents the mineral in question, the mineral precipitates; for $F_I=0$ chemical equilibrium exists and nothing happens; for $F_I>0$ the mineral dissolves, but only as long as the mineral exists, i.e., $\rho_I>0$.

Similarly, (35)–(37) give rise to the following set of rate equations associated with the aqueous species Ca^{2+}, SO_4^{2-}, Mg^{2+} and TIC involved in the precipitation/dissolution processes (1):

$$\frac{d[\phi C_{ca}]}{dt}=\phi\dot r_{ca}=\phi(\dot r_c+\dot r_g),$$

$$\frac{d[\phi C_{so}]}{dt}=\phi\dot r_{so}=\phi\dot r_g,$$

$$\frac{d[\phi C_{mg}]}{dt}=\phi\dot r_{mg}=\phi\dot r_m,$$

$$\frac{d[\phi C_{TIC}]}{dt}=\phi\dot r_{TIC}=\phi(\dot r_c+\dot r_m). \tag{42}$$

Remark 3. In the proposed model we consider the reaction rate coefficients k^c, k^g, and k^m as constant. As demonstrated in several works, see for example (Gledhill and Morse, 2006; Pokrovsky et al., 2009) which focus on calcite dissolution rates in Na–Ca–Mg–Cl synthetic brines, it is observed experimentally that the reaction rate constant more generally depend on various factors like brine composition, temperature, CO_2 partial pressure P_{co2}, and ionic strength. At the current stage, we do no attempts to include such finer mechanisms in the model.

Remark 4. In this work we have not done any comparisons of simulated mineral distributions to the experimentally produced distributions after flooding. In other words there is not enough information to determine both k_i and n_i in the rate expressions. We have assumed that $n_i=0.5$ and used the experiments to determine k_i.

3. The coupled flow and chemical reaction model

Generally, in order to describe a given species we must consider that it can be located in solution as a free ion or a complex, on the surface to preserve the charge balance, or stored in matrix as a mineral. For the core flooding experiments we consider the solution species will be transported in pore space and between the storage points by advection of the bulk phase, diffusion and dispersion of the species, chemical reactions between rock and fluid and equilibrium reactions. The purpose of this section is to derive the full transient model that accounts for all these effects.

3.1. Mass conservation

We need to take into account advective and diffusive forces associated with the brine in the pore space. In order to include such effects we must consider the following equations for the total concentrations ρ_c, ρ_g, ρ_m, ρ_l, ρ_{TIC}, ρ_{ca}, ρ_{so}, ρ_{mg}, ρ_{na}, ρ_{cl}:

$\partial_t(\rho_l)+\nabla\cdot(\rho_l\mathbf{v}_l)=0$ (water flowing through the pore space),

$\partial_t(\rho_{TIC})+\nabla\cdot(\rho_{TIC}\mathbf{v}_g)=\phi(\dot r_c+\dot r_m)$ (carbon as CO_2, HCO_3^- and CO_3^{2-} in water),

$\partial_t(\rho_{na}+\rho_{na}^s)+\nabla\cdot(\rho_{na}\mathbf{v}_g)=0$ (Na^+-ions in water and on rock surface),

$\partial_t(\rho_{cl})+\nabla\cdot(\rho_{cl}\mathbf{v}_g)=0$ (Cl^--ions in water),

$\partial_t(\rho_{ca}+\rho_{ca}^s)+\nabla\cdot(\rho_{ca}\mathbf{v}_g)=\phi(\dot r_c+\dot r_g)$ (Ca^{2+}-ions in water and on rock surface),

$\partial_t(\rho_{so})+\nabla\cdot(\rho_{so}\mathbf{v}_g)=\phi\dot r_g$ (SO_4^{2-}-ions in water),

$\partial_t(\rho_{mg}+\rho_{mg}^s)+\nabla\cdot(\rho_{mg}\mathbf{v}_g)=\phi\dot r_m$ (Mg^{2+}-ions in water and on rock surface),

$\partial_t(\rho_c)=-\phi\dot r_c$ (precipitation/dissolution of $CaCO_3$),

$\partial_t(\rho_g)=-\phi\dot r_g$ (precipitation/dissolution of $CaSO_4$),

$\partial_t(\rho_m)=-\phi\dot r_m$, (precipitation/dissolution of $MgCO_3$). (43)

Note that ρ_{na}^s, ρ_{ca}^s, and ρ_{mg}^s represent ion concentrations of species attached to the rock, as explained in Section 2.4. The first seven equations represent concentrations associated with the pore space, the last three equations are associated with the matrix. Here $\mathbf{v}_l$ and $\mathbf{v}_g$ are, respectively, the effective water and ion *fluid* velocities through the pores. They are related to the seepage velocities $\mathbf{V}_l$ and $\mathbf{V}_g$ by

$$\mathbf{V}_l=\phi\mathbf{v}_l,\quad \mathbf{V}_g=\phi\mathbf{v}_g. \tag{44}$$

Furthermore, we define the porous concentrations of the various components in water as the concentration taken with respect to the volume of the pores. The porous concentrations C_l, C_{TIC}, C_{na}, C_{cl}, C_{ca}, C_{so} and C_{mg} are related to the total concentrations by

$$\rho_i=\phi C_i,\quad (i=l,TIC,na,cl,ca,mg,so). \tag{45}$$

The seepage velocities are eliminated using the theory of Darcy's law concerning the entire water phase and diffusion concerning the components. The ions can be represented by the group

$$C_g=C_{TIC}+C_{na}+C_{cl}+C_{ca}+C_{mg}+C_{so}, \tag{46}$$

while the entire water phase is represented by

$$C=C_l+C_g. \tag{47}$$

The seepage velocity of the water phase, $\mathbf{V}$, is given by

$$C\mathbf{V}=C_g\mathbf{V}_g+C_l\mathbf{V}_l \tag{48}$$

and obeys Darcy's law

$$\mathbf{V}=-\frac{\kappa}{v}\nabla p, \tag{49}$$

where κ is the permeability of the porous medium, v is the fluid viscosity and p is the pressure. We define the diffusive velocity $\mathbf{U_g}$ as

$$\mathbf{U_g}=\mathbf{V_g}-\mathbf{V} \tag{50}$$

and can write the system of equations as

$$\partial_t(\phi C_l)+\nabla\cdot(C_l\mathbf{V}_l)=0,$$

$$\partial_t(\phi C_{TIC})+\nabla\cdot(C_{TIC}\mathbf{U}_g)+\nabla\cdot(C_{TIC}\mathbf{V})=\phi(\dot r_c+\dot r_m),$$

$$\partial_t(\phi C_{na}+\rho_{na}^s)+\nabla\cdot(C_{na}\mathbf{U}_g)+\nabla\cdot(C_{na}\mathbf{V})=0,$$

$$\partial_t(\phi C_{cl})+\nabla\cdot(C_{cl}\mathbf{U}_g)+\nabla\cdot(C_{cl}\mathbf{V})=0,$$

$$\partial_t(\phi C_{ca}+\rho_{ca}^s)+\nabla\cdot(C_{ca}\mathbf{U}_g)+\nabla\cdot(C_{ca}\mathbf{V})=\phi(\dot r_c+\dot r_g),$$

$$\partial_t(\phi C_{so})+\nabla\cdot(C_{so}\mathbf{U}_g)+\nabla\cdot(C_{so}\mathbf{V})=\phi\dot{r}_g,$$

$$\partial_t(\phi C_{mg}+\rho^s_{mg})+\nabla\cdot(C_{mg}\mathbf{U}_g)+\nabla\cdot(C_{mg}\mathbf{V})=\phi\dot{r}_m,$$

$$\partial_t\rho_c=-\phi\dot{r}_c,\quad \partial_t\rho_g=-\phi\dot{r}_g,\quad \partial_t\rho_m=-\phi\dot{r}_m. \tag{51}$$

3.2. Dispersion

The diffusive velocity is given by Ficks law which states that the flux is proportional to the concentration gradient:

$$C_i\mathbf{u_g}=\frac{C_i\mathbf{U_g}}{\phi}=-D\nabla C_i,\quad (i=TIC,na,cl,ca,so,mg), \tag{52}$$

where the diffusion coefficient is defined by the Perkins Johnston correlation (Green and Willhite, 1998) as

$$D=\left(\frac{D_m}{F_R\phi}+\frac{|\mathbf{v}|F_I d_p}{2}\right)I, \tag{53}$$

where D_m is the molecular diffusion coefficient, F_R is the formation resistivity factor, F_I the formation inhomogeneity factor and d_p the average particle diameter. F_R is correlated to porosity and lithology. Especially we assume $F_R=1/\phi^2$ as in Rider (2002) and that the product $\alpha=F_I d_p/2$ is constant. Then for a given seepage velocity and porosity the diffusion coefficient is

$$D(\phi,|V|)=\left(D_m\phi+\alpha\frac{|\mathbf{V}|}{\phi}\right)I. \tag{54}$$

The principal components of the tensor D are taken to be equal, meaning that diffusion behaves similarly in all directions.

3.3. The water equation

Summing the equations for all water components gives an equation for C instead of C_l. The sum is given by

$$\partial_t\left(\phi C+\sum_i\rho^s_i\right)+\nabla\cdot(C_l\mathbf{V}_l)-\nabla\cdot(D\phi\nabla C_g)+\nabla\cdot(C_g\mathbf{V})=2\phi(\dot{r}_c+\dot{r}_g+\dot{r}_m). \tag{55}$$

The second term can be rewritten using

$$\begin{aligned}C_l\mathbf{V}_l&=C\mathbf{V}-C_g\mathbf{V}_g=C\mathbf{V}-C_g(\mathbf{U}_g+\mathbf{V})\\&=\mathbf{V}(C-C_g)-C_g\mathbf{U}_g=C_l\mathbf{V}-C_g\mathbf{U}_g,\end{aligned} \tag{56}$$

simplifying the left side of the above equation as

$$\begin{aligned}&\partial_t\left(\phi C+\sum_i\rho^s_i\right)+\nabla\cdot(C_l\mathbf{V})-\nabla\cdot(C_g\mathbf{U}_g)-\nabla\cdot(D\phi\nabla C_g)+\nabla\cdot(C_g\mathbf{V})\\&\quad=\partial_t\left(\phi C+\sum_i\rho^s_i\right)+\nabla\cdot(C\mathbf{V})-(\nabla\cdot(C_g\mathbf{U}_g)+\nabla\cdot(D\phi\nabla C_g))\\&\quad=\partial_t\left(\phi C+\sum_i\rho^s_i\right)+\nabla\cdot(C\mathbf{V}).\end{aligned} \tag{57}$$

Thus the water component equation is replaced by a water phase equation:

$$\partial_t\left(\phi C+\sum_i\rho^s_i\right)+\nabla\cdot(C\mathbf{V})=2\phi(\dot{r}_c+\dot{r}_g+\dot{r}_m). \tag{58}$$

3.4. Porosity

It is now appropriate to define the local porosity in terms of the amount of minerals present at a given location. Per definition it is the volume fraction of rock that is porous volume. For each mineral we know the molar weight M_i (g/mol) and density ω_i (g/l) as relatively constant parameters (see Appendix C.1). The volume fraction of one mineral is

$$\frac{M_i}{\omega_i}\rho_i\quad (i=c,g,m). \tag{59}$$

We thus define the porosity as 1 minus the volume fractions of minerals:

$$\phi(\rho_c,\rho_g,\rho_m)=1-\frac{M_c}{\omega_c}\rho_c-\frac{M_g}{\omega_g}\rho_g-\frac{M_m}{\omega_m}\rho_m. \tag{60}$$

We arrive at a model of the form

$$\partial_t\left(\phi C+\sum_{i:cations}\rho^s_i\right)+\nabla\cdot(C\mathbf{V})=\phi(\dot{r}_c+2\dot{r}_g+\dot{r}_m),$$

$$\partial_t(\phi C_{TIC})-\nabla\cdot(D\phi\nabla C_{TIC})=\phi(\dot{r}_c+\dot{r}_m)-\nabla\cdot(C_{TIC}\mathbf{V}),$$

$$\partial_t(\phi C_{na}+\rho^s_{na})-\nabla\cdot(D\phi\nabla C_{na})=-\nabla\cdot(C_{na}\mathbf{V}),$$

$$\partial_t(\phi C_{cl})-\nabla\cdot(D\phi\nabla C_{cl})=-\nabla\cdot(C_{cl}\mathbf{V}),$$

$$\partial_t(\phi C_{ca}+\rho^s_{ca})-\nabla\cdot(D\phi\nabla C_{ca})=\phi(\dot{r}_c+\dot{r}_g)-\nabla\cdot(C_{ca}\mathbf{V}),$$

$$\partial_t(\phi C_{so})-\nabla\cdot(D\phi\nabla C_{so})=\phi\dot{r}_g-\nabla\cdot(C_{so}\mathbf{V}),$$

$$\partial_t(\phi C_{mg}+\rho^s_{mg})-\nabla\cdot(D\phi\nabla C_{mg})=\phi\dot{r}_m-\nabla\cdot(C_{mg}\mathbf{V}),$$

$$\partial_t\rho_c=-\phi\dot{r}_c,\quad \partial_t\rho_g=-\phi\dot{r}_g,\quad \partial_t\rho_m=-\phi\dot{r}_m,$$

$$\mathbf{V}=-\frac{\kappa}{v}\nabla p,$$

$$D=\left(D_m\phi+\alpha\frac{|\mathbf{V}|}{\phi}\right)I,$$

$$\phi=1-\frac{M_c}{\omega_c}\rho_c-\frac{M_g}{\omega_g}\rho_g-\frac{M_m}{\omega_m}\rho_m. \tag{61}$$

Note that permeability only appears in the expression for $\mathbf{V}$. It could be relevant to let it vary with porosity or mineral composition, but it is only the value of $\mathbf{V}$ which matters for the solution. The experiments are performed with pressure regulated to keep a certain volume injection rate. Any change in κ is compensated by a change in pressure. With the given setting it is therefore not relevant to consider anything but a constant permeability.

3.5. Simplifying assumptions

So far we have made the following simplifications of the chemistry

- Only three minerals are present: calcite, magnesite, anhydrite.
- P_{co2} is brine- and temperature-dependent, but constant during a flooding.
- The fraction of uncomplexed ions is ion-, brine- and temperature-dependent, but constant during flooding.
- The pH is in a range such that we can neglect CO_3^{2-} in the charge balance.
- The temperature during flooding is constant.

We will now proceed by simplifying the transport system:

- Assuming now that the water phase is incompressible we can set C constant.
- For simplicity we also assume that the mass transferred from the reactions that adds to the water phase volume (from dissolved minerals or ions released from the surface) exactly balances with the expansion of the pore space. In other

words, the chemical reactions do not accelerate or decelerate the fluid by altering the volume. In mathematical terms it then follows from (58) that:

$$\nabla \cdot \mathbf{V} = 0 \quad \Leftrightarrow \quad \mathbf{V} = -\frac{\kappa}{\nu}\nabla p \quad \text{is uniform.} \tag{62}$$

The velocity can depend on time, but is uniform in a given direction according to this assumption. Consequently, the water phase equation is eliminated.

- The model can be further simplified by assuming constant porosity, velocity and diffusion coefficient. It is a fair approximation to the real solution as long as the porosity is close to uniform and does not change too much with time. However, even if porosity is assumed constant in the equations we get an estimate of how it varies from (60) given by the solution for the mineral concentrations.
- The carbon equation, second equation of (61), is ignored as we assume a constant partial pressure of CO_2 that depends on the injected brine, see Section 2.3. The implication is a constant concentration of CO_2. Concentrations of other carbon species are determined by this P_{co2} and the pH. The motivation for this approximation is that for these experiments there is little variation in the pH (≈ 2 units from inlet to outlet) and also the *TIC* seems to change little (especially in the $MgCl_2$ case) such that the P_{co2} should not change too much. Thus, the mathematical formulation is simplified in the sense that we calculate the most relevant equilibrium chemistry by simple formulas (A.14) instead of frequently finding solutions to algebraic iteratively.

Consequently the unknown variables we solve for are C_{na}, C_{cl}, C_{ca}, C_{so}, C_{mg}, ρ_c, ρ_g and ρ_m. Note that from the model (61) we obtain $\rho_i^{tot} = \rho_i + \rho_i^s = \phi C_i + \rho_i^s$ for $i = na,ca,mg$ and $\rho_j^{tot} = \rho_j = \phi C_j$ for $j = cl,so$. Then, following the procedure outlined in Section 2.4 we can obtain C_i and ρ_i^s for the various ions i. We also refer to Appendix B for more details how the different variables are found through the numerical solution procedure.

3.6. Scaling the system

In the following we restrict ourselves to a one-dimensional version of the model (61) which is indeed a reasonable approximation in the context of core flooding experiments. We also want to scale the system so that all quantities, with the exception of the concentrations above, are expressed relative to a reference value.

Let τ be the time scale of the problem. An appropriate space scale is given by the length of the core, L. We choose a reference diffusion coefficient as

$$\overline{D} = \frac{L^2}{\tau}. \tag{63}$$

We then define dimensionless independent variables as follows:

$$x' = \frac{x}{L}, \quad t' = \frac{t}{\tau}, \tag{64}$$

and dimensionless coefficients

$$D'_m = \frac{D_m}{\overline{D}}, \quad D' = \frac{D}{\overline{D}}, \quad \kappa' = \frac{\kappa}{\overline{\kappa}}, \quad p' = \frac{p}{\overline{p}}, \tag{65}$$

where $\overline{p}$ is a reference pressure, $\overline{\kappa}$ is reference permeability, and $\overline{D}$ reference diffusion coefficient. From the definition of Darcy's law and the diffusion coefficient we have

$$V = -\frac{\kappa}{\nu}\frac{\partial p}{\partial x} = -\frac{\overline{\kappa}\overline{p}}{\nu\overline{D}}\frac{L}{\tau}\frac{\kappa'\partial p'}{\partial x'},$$

$$D = D_m\phi + \alpha\frac{|V|}{\phi} = \overline{D}\left(D'_m\phi + \frac{\alpha}{L\phi}\left|-\frac{\overline{\kappa}\overline{p}}{\nu\overline{D}}\frac{\kappa'\partial p'}{\partial x'}\right|\right). \tag{66}$$

We introduce the parameters

$$\varepsilon = \frac{\overline{\kappa}\overline{p}}{\nu\overline{D}}, \quad \mu = \frac{\alpha}{L}. \tag{67}$$

We can then define a scaled velocity J and diffusion coefficient as

$$J(t) := \frac{V(t)}{L/\tau} = -\varepsilon\frac{\kappa'\partial p'}{\partial x'}, \tag{68}$$

$$D' = D'_m\phi + \frac{\mu|J|}{\phi}. \tag{69}$$

The velocity is determined from known information about the injection rate. The t-dependency accounts for possible variations in the injection rate as time is running.

Now let Q be the injection rate, measured in m^3/s and let q be the injection rate expressed in pore volumes per day, PV/d. We set $\tau = 1d = 24 \times 3600$ s. Then

$$Q[m^3/s] = q[PV/d]\frac{AL\phi_{in}[m^3/PV]}{\tau[s/d]}, \tag{70}$$

where A is the area of an intersection of the core, L is length of the core, and τ is the reference time. Here PV refers to the initial pore volume, as defined by the initial overall porosity ϕ_{in}. Q can also be expressed as

$$Q = AV = A\frac{L}{\tau}J. \tag{71}$$

Combining (70) and (71) results in

$$J = q\phi_{in}. \tag{72}$$

The interpretation of this is that if we inject with a possibly varying rate $q(t)$ over time, then the scaled velocity used in solving the system is given by $J(t)$.

The model (61), when we apply the assumptions specified in Section 3.5 and introduce the dimensionless variables (64) and (65), takes the form (where the prime notation is skipped)

$$\partial_t(\phi C_{na} + \rho_{na}^s) + \partial_x(C_{na}J) = \partial_x(D\phi\partial_s C_{na}),$$

$$\partial_t(\phi C_{cl}) + \partial_x(C_{cl}J) = \partial_x(D\phi\partial_x C_{cl}),$$

$$\partial_t(\phi C_{ca} + \rho_{ca}^s) + \partial_x(C_{ca}J) = \tau\phi(\dot{r}_c + \dot{r}_g) + \partial_x(D\phi\partial_s C_{ca}),$$

$$\partial_t(\phi C_{so}) + \partial_x(C_{so}J) = \tau\phi\dot{r}_g + \partial_x(D\phi\partial_x C_{so}),$$

$$\partial_t(\phi C_{mg} + \rho_{mg}^s) + \partial_x(C_{mg}J) = \tau\phi\dot{r}_m + \partial_x(D\phi\partial_x C_{mg}),$$

$$\partial_t\rho_c = -\tau\phi\dot{r}_c,$$

$$\partial_t\rho_g = -\tau\phi\dot{r}_g,$$

$$\partial_t\rho_m = -\tau\phi\dot{r}_m, \tag{73}$$

where D, J, ϕ and τ are constant. Note that the reaction terms $\dot{r}_c$, $\dot{r}_g$, and $\dot{r}_m$, in view of (39)–(42), are functions of C_{na}, C_{cl}, C_{ca}, C_{so}, C_{mg}, ρ_c, ρ_g and ρ_m.

3.7. Initial and boundary conditions

The model (73) must be equipped with appropriate initial conditions:

$$C_i|_{t=0} = C_i^0(x) \quad (i = na,cl,ca,so,mg),$$

$$\rho_j|_{t=0} = \rho_j^0(x) \quad (j = c,g,m),$$

$$\rho_k^s|_{t=0} = \rho_k^{s,0}(x) \quad (k = na,ca,mg), \tag{74}$$

and Dirichlet boundary conditions at the left end of the domain

$$C_i|_{x=0} = C_i^L \quad (i = na,cl,ca,so,mg), \tag{75}$$

where the brine with a known concentration of the different ions is injected into the core plug. The right side boundary is determined using a zero concentration gradient condition:

$$\partial_x C_i|_{x=1} = 0 \quad (i = na,cl,ca,so,mg). \tag{76}$$

For the numerical approach we use to solve the system of advection–diffusion–reaction equations we refer to Appendix B.

4. Numerical investigations

The purpose of this section is to provide a detailed comparison of the model predictions and the experimental results when we consider flooding of chalk cores for a series of different brines. We emphasize that the different model parameters related to transport effects (injection rate and dispersion, see (80)) and chemical reactions (reaction rate constants, solubility products, equilibrium constants and ionic parameters, see (79), Appendices C.2 and C.3) are kept unchanged for the different examples.

A chief objective of this work is to discuss the *combined* effect of dissolution/precipitation and ion exchange. The model employed in Evje et al. (2009) and Madland et al. (2011) only accounted for dissolution/precipitation and could not explain the transient behavior in the initial stage of the flooding experiments as explained and illustrated in the introduction, see Fig. 3. Thus, after tuning transport and reaction kinetic parameters in Section 4.3, we take into account the ion exchange processes in Section 4.4. This will demonstrate how the transient variations in effluent concentrations can be captured.

Section 4.5 shows some predictions of profiles of ions, minerals and surface composition along the core for flooding with $MgCl_2$. These quantities are of interest, in particular, for further studies where changes in these quantities presumably play a role in the context of brine-dependent oil recovery (Evje and Hiorth, 2010, 2011) and brine-dependent stress–strain behavior (Madland et al., 2011). Finally, Section 4.6 gives a discussion concerning sensitivity to grid refinement and the choice of splitting step Δt.

4.1. Experimental setup

The experimental results we refer to in this section is based on some recent experiments reported in Madland et al. (2011). Outcrop chalk from a quarry near Liege in Belgium was used in the experimental work. This chalk is composed of approximately 98% calcite and 2% other non-carbonate minerals. The motivation for these experiments was to select a repeatable type of tests in order to gain further in depth understanding behind the mechanisms causing the water-weakening of chalks. Hydrostatic- and creep tests with continuous flooding of various fluids, at an injection rate equal to approximately 1 pore volume per day (1 PV/D), were performed in a standard hydraulically operated triaxial cell equipped with a heat regulating system. During the experiments the temperature was kept constant; 130 °C.

In the following we shall compare the model to experimental results where chalk cores were flooded, respectively, with NaCl, $MgCl_2$ and seawater. Two different concentrations of $MgCl_2$ were considered corresponding to different ionic strength. Also, two different seawater-like brines were applied where the main difference was the ionic strength. See Table C3 in Appendix C.4 for details about the different brines that were considered.

In our model the brines were constructed using the assumedly most reactive ions (Ca^{2+}, SO_4^{2-}, Mg^{2+}) and those contributing to the ionic strength (Na^+, Cl^-). In practice the brines are constructed by dissolving a mixture of the salts NaCl, Na_2SO_4, $NaHCO_3$, KCl, $MgCl_2 \times 6H_2O$ and $CaCl_2 \times 2H_2O$. K^+ behaves inert and appeared in small amounts so we decided to treat KCl as NaCl as this species was not included in the model.

The pH calculation is quite sensitive to any deviance in the charge balance. Therefore it is preferable to state a composition based on the salts used and not the individual ions. As an example, using (A.14) to calculate the pH for seawater SSW-I gives the extremely low 2.15 when K^+ is neglected in the brine composition (see Appendix C.4) instead of replacing with Na^+. Restoring the charge balance with Na^+ produces a pH of 8.50 which is reasonably close to the calculation by PHREEQC (Parkhurst and Appelo, 1999) of 8.23.

In these tests the cores were hydrostatically or isotropically loaded beyond yield and thereafter left to creep at a constant stress level of 10.5 MPa. Sampling of the effluent was continuously conducted during the hydrostatic phase as well as during the following creep phase. The effluent was chemically analyzed in order to quantify any chemical changes of the core material.

4.2. Input data for the model

We consider a core of length $L=0.07$ m with porosity $\phi = 0.48$. The brines are mixed at $T^{atm}=25$ °C, while the flooding is performed at $T^{res}=130$ °C. The molecular diffusion coefficient D_m is assumed constant. From data in Lasaga (1998) extrapolated to 130 °C and averaged for the ions we get $D_m = 3.5 \times 10^{-9}$ (m^2/s). Numerically we discretize the core into 60 cells and use a splitting step of $\Delta t = 1$ h. The reference time is $\tau = 1$ day $= 24 \times 3600$ s. Equilibrium constants and parameters for species and brines are listed in Appendices C1, C2 and C3.

Based on the given input we calculate a reference diffusion coefficient as $\overline{D} = L^2/\tau = 5.67 \times 10^{-8}$ (m^2/s) and scale the molecular diffusion in (69): $D'_m = 0.062$ (dimensionless).

4.2.1. Initial concentrations

As initial data for the simulations we assume a core composed of the mineral $CaCO_3$. From the definition of porosity (60) we can derive the initial concentration of calcite if there are no impurities:

$$\rho_c^0 = (1-\phi_{in})\frac{\omega_c}{M_c} = 14.08 \text{ (mol/l)}. \tag{77}$$

More precisely, the following total concentrations (mol/l) are given initially for the minerals associated with the core

$$\rho_c^0 = 14.08, \quad \rho_g^0 = 0, \quad \rho_m^0 = 0 \text{ (mol/l)}.$$

Moreover, it is assumed that the core is initially filled with pure water, in other words, all ion concentrations are set to zero inside the core.

$$C_i^0 = 0 \quad (i = na,cl,ca,so,mg).$$

The first step in the calculations is to find updated concentrations such that the system is in thermodynamical equilibrium before we start the flooding. Practically speaking, for the chemical system we consider this gives a very small correction of the order of $O(10^{-3})$ for the Ca^{2+} concentration and a corresponding dissolution of calcite, $CaCO_3$.

In Section 4.3 we will assume $CEC=0$ such that

$$\rho_i^{s,0} = 0 \quad (i = na,ca,mg).$$

Later, in Section 4.4 we include a nonzero $CEC > 0$. It is then assumed that the surface initially stores only Ca^{2+}-ions. That is because the cores initially were flooded with a few pore volumes of distilled water and the only cations available would then be Ca^{2+} from calcite. Initial conditions for the surface are then

given as:

$$\rho_{ca}^{s,0} = CEC/2(\text{mol/l}) \quad \Leftrightarrow \quad \beta_{ca}^{0} = 1. \tag{78}$$

4.3. Examples without effect of ion exchange

The examples of this section are used to illustrate some key elements:

- Advection and dispersion are important transport mechanisms in the given setup;
- There is a loss or gain of different ions in the effluent compared to the injected brine;
- As injection begins a transient effluent is observed which develops into a steady state;
- We will use the mechanism of mineral dissolution/precipitation to explain the steady state behavior and history match the reaction kinetic parameters;
- The transient period differs significantly from the predictions indicating that more mechanisms than just dissolution/precipitation are present.

4.3.1. Experimentally determined parameters

Parameters for advection, diffusion, and reaction are chosen as follows:

$$k^c = 3.5 \times 10^{-6}, \quad k^g = 0.075k^c, \quad \text{and} \quad k^m = 0.09k^c \quad (\text{mol/l})/\text{s}$$

$$n_c = n_g = n_m = 0.5, \tag{79}$$

$$D = 8 \times 10^{-8}(\text{m}^2/\text{s}) \Leftrightarrow D' = 1.4, \quad q = 1.0, \quad \alpha = 0.097\ (\text{m}), \tag{80}$$

where q is given by (72) and D represents the combined effect of molecular diffusion and mechanical dispersion as described by (69). More information about the estimation of these parameters, based on the experimental results, are given below. In particular, we note that having estimated D (total dispersion effect) it is possible to determine the parameter α in the dispersion coefficient from (69) and (72).

4.3.2. Example 1: NaCl

At first, we consider a brine with a concentration of 0.657 M NaCl (see Table C3) that is injected into a chalk core at the left inlet with the constant rate of 1 PV/d which corresponds to $q=1$.

The results in terms of measured ion concentrations of the effluent are shown in Fig. 4. The fact that the produced concentrations of Na^+ and Cl^- reach and maintain the injected concentration values shows that it is reasonable to assume these ions are not participating in water–rock chemistry in terms of dissolution or precipitation.

The Na^+ effluent arrives later than that of Cl^- and a natural interpretation is that this is due to adsorption of Na^+-ions. The diffusion coefficient D is therefore matched using the Cl^- profile since this ion seems to behave inert. The resulting value is given by (80).

Along with the adsorption of Na^+ there is an observed release of Ca^{2+} which indicates that the cations are exchanged. This is not just the dissolved calcite initially in solution because the observed high concentration of 0.04 mol/l is much greater than the calcium concentration of (atmospherically carbonated) distilled water in equilibrium with calcite (0.002 mol/l as estimated both by PHREEQC and this model). Also, the Ca^{2+}-profile stabilizes at a level greater than zero, indicating some dissolution is taking place.

To conclude, assuming a system controlled by advection and dispersion we are then able to capture the Cl^- profile, however, the Na^+ profile and Ca^{2+} profile require more mechanisms for a full explanation. We shall return to this discussion in Section 4.4.

4.3.3. Example 2: $MgCl_2$ brines

In this example we will consider two flooding cases with $MgCl_2$, the only difference being the concentrations: 0.109 and 0.219 M. Compositions are given in Appendix C.4. We wish to match the steady state concentrations in the effluent by adjusting reaction rate parameters. First, we selected a value for k_c and next adjusted the value of k_m to fit the profiles.

Example 2a: 0.109 M $MgCl_2$

From Fig. 5, the following observations are made:

- After some time (approximately 7 days) a steady state like solution seems to have been reached. The calculated concentration profiles fit well with the experimental concerning the steady state level.
- The experimental concentration profiles reflect that there is a loss of Mg^{2+} ions inside the core (the effluent stabilizes below the injected value) and a corresponding production of Ca^{2+} ions (the sum of produced Ca^{2+} and Mg^{2+} equals the injected value of Mg^{2+}).

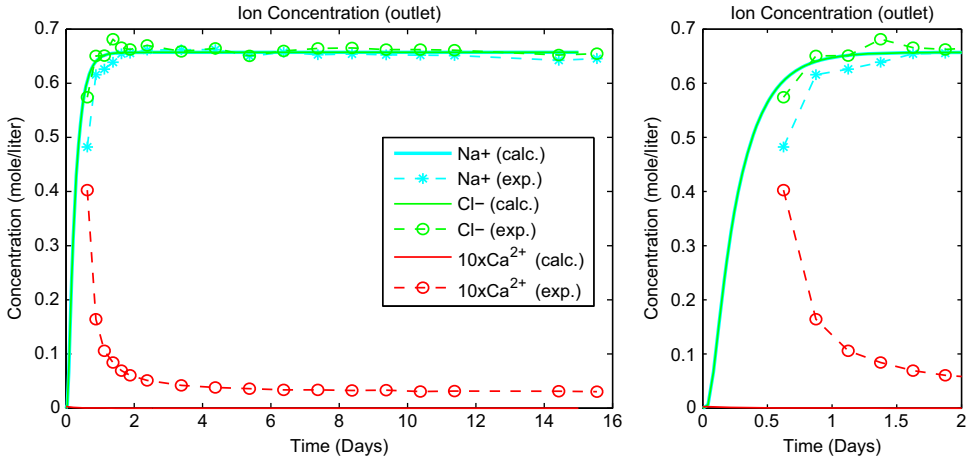

Fig. 4. History matching the flooding of NaCl to determine dispersion coefficient D and demonstrate ion exchange. Calculated profiles are based on advection and dispersion only. Therefore calculated Na^+ and Cl^- profiles overlap. Note that Ca^{2+}-profile is scaled up for visibility.

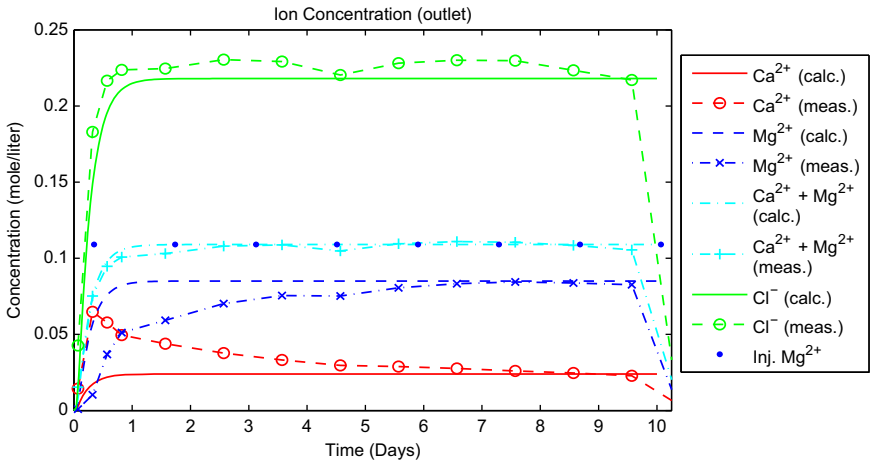

Fig. 5. Effluents after injection of 0.109 M $MgCl_2$. Concentrations at outlet for various ions, Ca^{2+}, Mg^{2+}, and Cl^-. Comparison between experimental results and calculated solutions of the model.

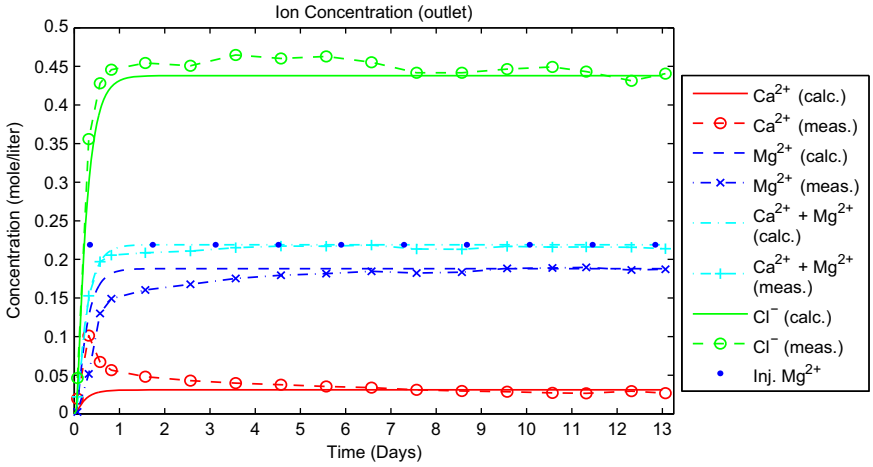

Fig. 6. Effluents after injection of 0.219 M $MgCl_2$. Concentrations at outlet for various ions, Ca^{2+}, Mg^{2+}, and Cl^-. Comparison between experimental results and calculated solutions of the model.

- There is a discrepancy between experimental and calculated concentrations in the initial period. More precisely, there is a strong production of Ca^{2+} ions in the very beginning, and a corresponding strong consumption of Mg^{2+} ions not captured by the model. One possibility could perhaps be that the reaction rate constants are not constant, see Remark 3 and references therein. However, in the next section we will propose an explanation based on incorporation of ion exchange effects.

Example 2b: 0.219 M $MgCl_2$

In this example we have doubled the concentration of $MgCl_2$, i.e., a water mixture with 0.219 mol $MgCl_2$ is injected at the left inlet with the same constant rate. The resulting concentration profiles, both experimental and computed, are shown in Fig. 6.

Most interestingly, we observe that the steady state levels of the ion concentrations measured at the outlet fit well with the computed concentrations. In particular, the relatively strong alteration in consumed Mg^{2+} ions from Example 2a to Example 2b is nicely captured (the loss of Mg^{2+} goes from 0.024 mol/l to 0.031 mol/l).

Also for this test there is a high production of Ca^{2+} and consumption of Mg^{2+} during the initial stages. In particular, the peak in the Ca^{2+} effluent is twice as high in the case with double $MgCl_2$ concentration, indicating a strong brine dependence. The sum of Ca^{2+} and Mg^{2+} concentrations again reach that of the injected value, indicating that precipitation/dissolution for a Ca^{2+}–Mg^{2+} -system behaves in a substitution-like manner.

4.3.4. Example 3: seawater-like brines

In this example two seawater-like brines are injected through a chalk core. SSW-I has a composition representative of normal seawater, while SSW-II has lower ionic strength, but the same concentration of Ca^{2+}, Mg^{2+} and SO_4^{2-} (see Appendix C.4). Unfortunately the test with SSW-I produced few measurements due to plugging of the core.

Given the reaction parameters k_c and k_m from the previous example the final reaction parameter k_g was estimated to best fit the steady state effluents of these two flooding experiments.

Example 3a: SSW-I synthetic seawater

From Fig. 7 it is seen that the effluent of both Ca^{2+} and Mg^{2+} have not stabilized properly and the predicted curves have compensated for this. However, it can be seen that there is a loss of Mg^{2+} and a gain in Ca^{2+}. The SO_4^{2-} effluent shows more stability and clearly demonstrates a loss of ions to the core which can be explained by the model as a consequence of precipitation

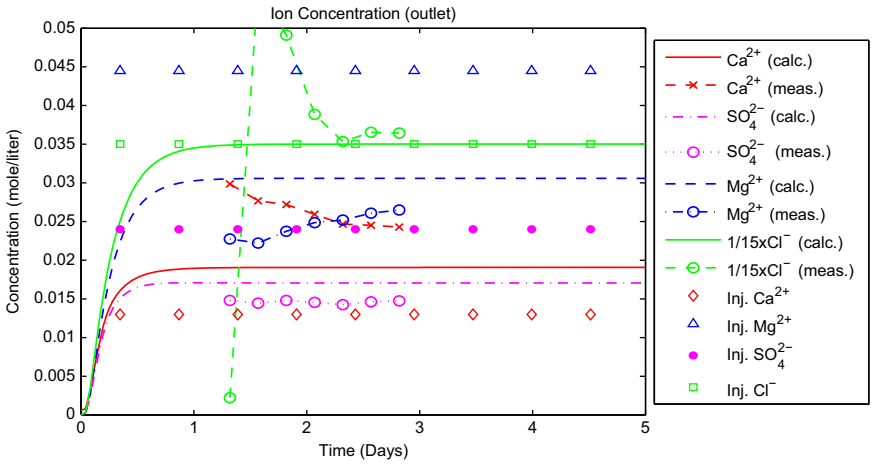

Fig. 7. Effluents after injection of SSW-I. Concentrations at outlet for various ions, Ca^{2+}, Mg^{2+}, and Cl^-. Comparison between experimental results and calculated solutions of the model. Note that Cl^- has been scaled for better visualization.

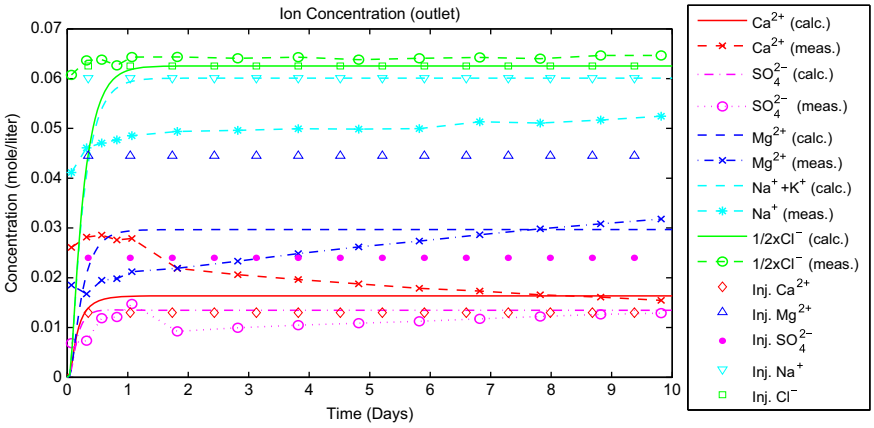

Fig. 8. Effluents after injection of SSW-II. Concentrations at outlet for various ions, Ca^{2+}, Mg^{2+}, and Cl^-. Comparison between experimental results and calculated solutions of the model. The measured curve for Na^+ is different from the predicted curve of $Na^+ + K^+$, because there is a concentration of 0.01 M K^+ in the seawater.

of anhydrite. Concerning the Cl^- effluent there were some measurement errors initially, but it stabilizes around the injected concentration again showing that it is an inert ion regarding precipitation/dissolution.

Example 3b: SSW-II synthetic seawater with low ionic strength

For this test the seawater-brine SSW-II was used. The results shown in Fig. 8 are similar to SSW-I in the sense that Ca^{2+} is produced, while Mg^{2+} and SO_4^{2-}-ions are lost. A specific feature of this test is that we see a more pronounced transient behavior that can be separated into two regions: an initial phase from 0 to 2 days where changes occur rapidly followed by a period where the effluent changes slowly. It does not seem to have fully converged to a steady state.

Looking at the numbers of the last measurements we see there is a gain of 0.0025 mol/l Ca^{2+}, a loss of 0.0125 mol/l Mg^{2+} and a loss of 0.011 mol/l SO_4^{2-}. Unlike the cases with $MgCl_2$, where the loss was equal to the gain, we see here that the loss is almost 10 times as high as the gain. In other words, we should expect plugging of the core after some time. This is also predicted by the model and observed in the laboratory experiments.

4.4. The effect of ion exchange

Now we want to take into account ion exchange in the model and see how this can improve the model predictions. As already mentioned we assume that Ca^{2+} is the only cation initially stored on the surface. The parameters for ion exchange we will use are

$$CEC = 0.4 \text{ (eq/l rock)}, \tag{81}$$

$$K^{chalk}_{na/ca}(130\ ^\circ\text{C}) = 0.042 \quad K^{chalk}_{na/mg}(130\ ^\circ\text{C}) = 0.055. \tag{82}$$

The reasoning behind this choice is as follows:

- The capacity *CEC* was determined by considering the transient phase of the $MgCl_2$ flooding of Example 2. The exchange constants $K^{soil}_{na/ca}, K^{soil}_{na/mg}$ listed in Appendix C.3 were based on soils or clays. As calcite is a very different material these values were only taken as an initial guess. Equipped with these exchange constants we found an optimal *CEC* by matching the transient phase, see Fig. 9. The best match is given by (81).
- Given the CEC and the initial choice of exchange constants $K^{soil}_{na/ca}, K^{soil}_{na/mg}$ we revisited the NaCl test, Example 1. The calculated solution gave a high peak for the Ca^{2+}-ions which suggested some tuning was necessary. The exchange constants $K^{soil}_{na/ca}, K^{soil}_{na/mg}$ were reduced by a factor 20 and the resulting values were denoted as $K^{chalk}_{na/ca}, K^{chalk}_{na/mg}$, see (82). As seen in Fig. 10 this gave a good match of the Ca^{2+} peak, the separation between Na^+ and Cl^-, as well as the steady state values. Note also that by altering the constants with the same factor we do not alter the way Ca^{2+} and Mg^{2+} distribute relatively. Hence, the above $MgCl_2$ simulations remain unchanged using (82).
- The given parameters (81) and (82) were then used to study the effect of including ion exchange for the flooding

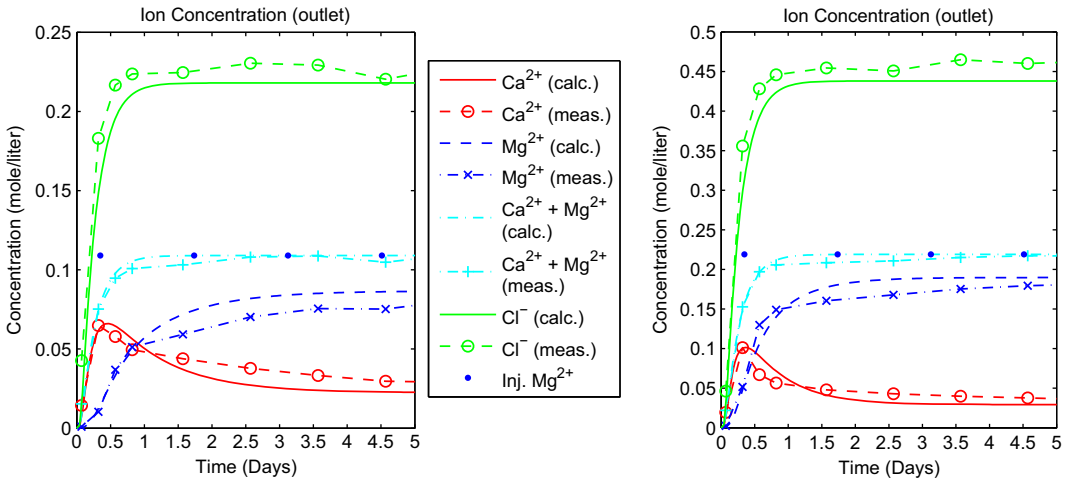

Fig. 9. Result of matching CEC with transient phase of low (left) and high (right) concentration $MgCl_2$ flooding. The early transient phase (0–2 days) is well captured in terms of Ca^{2+} peak and Mg^{2+} adsorption. The following slow transient before steady-state is improved.

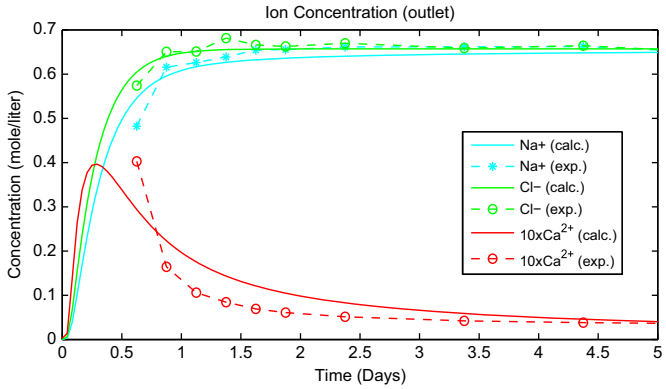

Fig. 10. Result of matching the exchange constants to the NaCl experiment with focus on the transient stage.

experiments with the more complicated seawater-like brines, see Fig. 11. It turned out to give a very good match and thereby served as a justification of the choice of these constants.

Considering the match with experimental data, illustrated in Figs. 9–11 with focus on the transient data, we can summarize a few observations:

- Assuming some initial Ca^{2+} on the surface implies that flooding with a brine containing Mg^{2+} or Na^{+} will induce a release of Ca^{2+} and adsorption of the other cations. This explains the transient Ca^{2+} peak in the effluent and the slow increase to a steady state for Mg^{2+}.
- The shape of the transient is brine-dependent. A very concentrated solution will displace much of the ions in very short time and give a high peak compared to the tail. As the concentration of $MgCl_2$ was doubled, less brine was required to fill the surface with Mg^{2+}. More Ca^{2+} was desorbed at one time, explaining the greater peak.
- After the transient stage a steady state develops. Since the brine composition along the core then does not change in time there is no more adsorption/desorption by ion exchange and therefore ion-exchange has no effect on the final steady-state, only the transient behavior.
- The simultaneous adsorption of Na^{+} and release of Ca^{2+} during NaCl flooding, see Fig. 10, indicates that Na^{+} plays a role on the surface of chalk, but is only weakly attracted. The surface favors adsorption of Ca^{2+} and Mg^{2+} as given by the optimal exchange constants.
- Seawater floodings (see Fig. 11) show a calculated transient behavior also for SO_4^{2-}: the concentration increases slowly towards a steady state. This is partly explained by the high concentrations of Ca^{2+} resulting from dissolution and ion exchange that give higher precipitation of anhydrite. Because of this Ca^{2+} and SO_4^{2-} mostly have opposite going trends. However, for SSW-II, very early there is an observed fall in SO_4^{2-} followed by a slow approach towards steady-state. This is not seen for SSW-I and is not captured by the model. As mentioned in the introduction SO_4^{2-} is known to be reactive towards the chalk surface. It may seem that an adsorption of SO_4^{2-} begins for SSW-II after 1.0 days. As a steady state is reached quite early for SSW-I this observation could be related to the difference in salinity. Wettability alteration in chalk is believed to be coupled to adsorption of sulfate. Furthermore, positive effects on oil recovery are also seen by reducing the salinity by NaCl (Fathi et al., 2011). It is therefore potentially interesting to note that a reduction in NaCl may induce increased adsorption of sulfate.

4.5. Changes along the core

When a brine is first injected there is a front that displaces the initial water, which is in equilibrium, and replaces it with reactive brine. This will change the composition on the rock surface, in the pore volume and perhaps alter the mineral content. As the injected water is farthest away from equilibrium we expect to see the highest gradients at the inlet point, while the travel along the core will make it less reactive.

To illustrate the changes along the core and in time we consider the case of flooding with 0.109 M $MgCl_2$ for 5 days. An initial surface composition of only Ca^{2+}-ions and a *CEC* of 0.30 (eq/l) is used.

Ion distribution

The resulting ion distribution along the core is pictured in Fig. 12. As seen in the first plot (for Ca^{2+}-ions) there is a wave of ions released into the solution from the rock as the injected $MgCl_2$

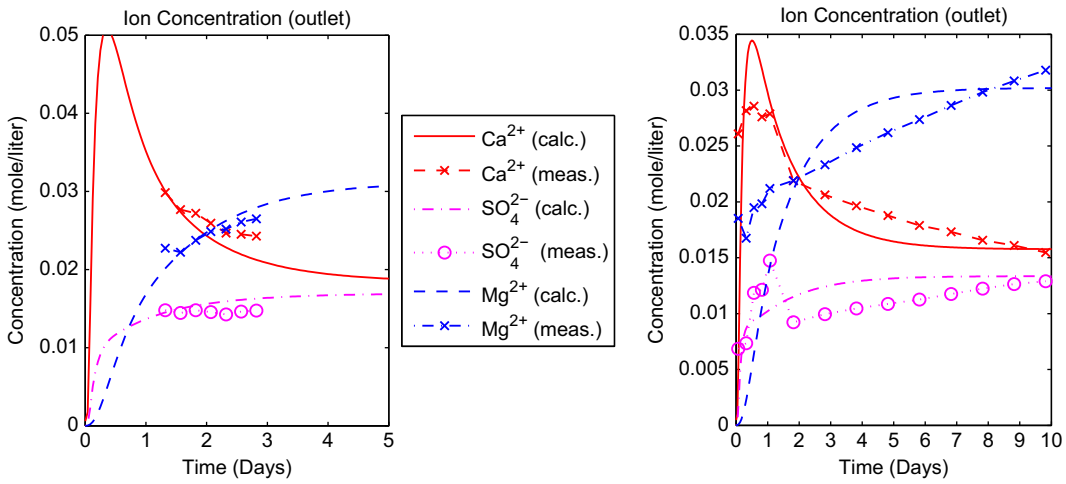

Fig. 11. Seawater tests modeled with ion exchange, advection/dispersion and precipitation/dissolution reactions. Left: SSW-I. Right: SSW-II.

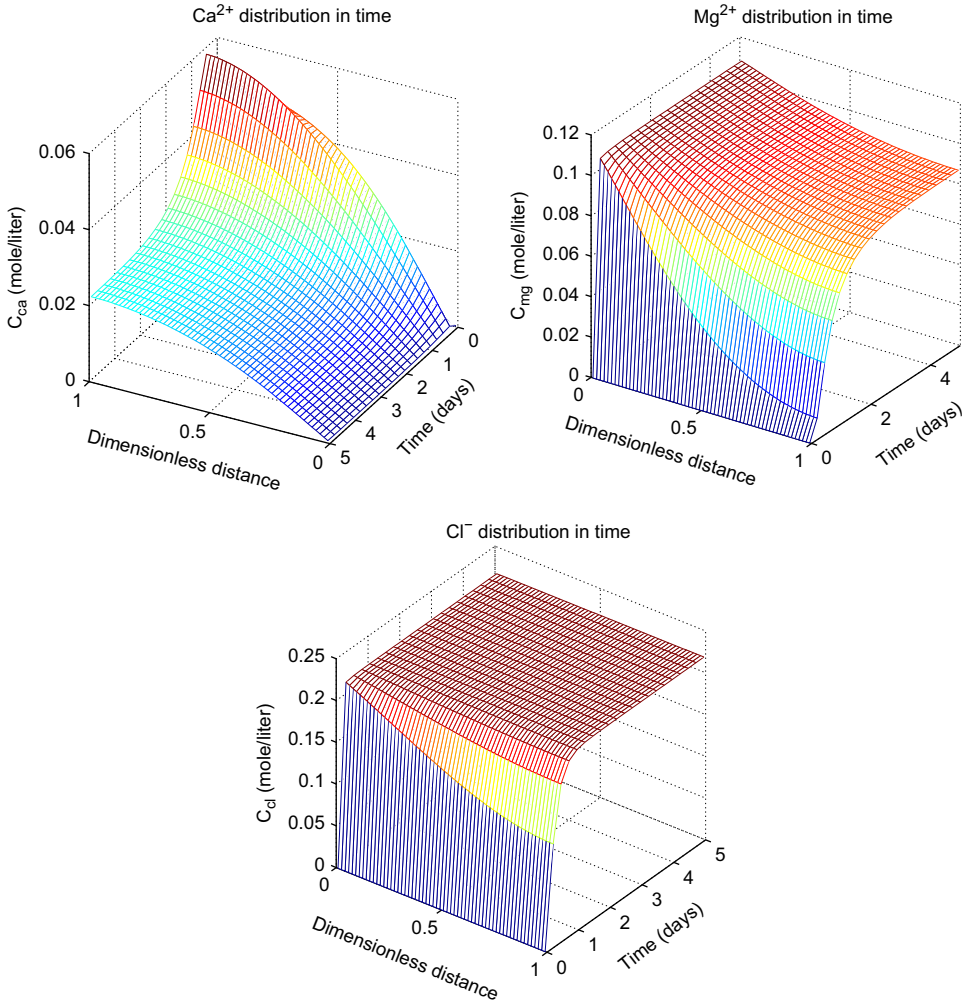

Fig. 12. 3D visualization of the ion distribution in time for 0.109 M $MgCl_2$.

exchanges Ca^{2+} for Mg^{2+}. After roughly 3 days the distribution along the core does not change any more with time, indicating that steady state has been achieved. The concentration increases gradually from inlet to outlet due to the dissolution of calcite. Ion exchange is manifested by the peak close to the outlet and seen during the first 2–3 days.

As seen in the second plot there is a consumption of Mg^{2+} along the core that causes the Mg^{2+} concentration to decrease. This is explained both by magnesite precipitation and ion exchange. Comparing with the third plot for Cl^- we see that the Mg^{2+}-ions take a longer time to reach a steady state. This difference can be ascribed to the effects of ion exchange.

Regarding the Cl^- distribution note that the steady state is a flat line along the core, meaning that there is no loss or gain along the core. The distribution quickly reaches this state because it is unaffected by the ion exchange process.

Surface distribution

Due to the equilibrium assumption for the surface composition there will be a change on the surface related to the injection of the new brine. This is represented by the equivalents fractions β for Ca^{2+} and Mg^{2+} in Fig. 13.

As seen by the first plot for surface bound Ca^{2+} the fraction β_{ca} is initially uniformly 1. It quickly decreases in time as Ca^{2+} is released and Mg^{2+} is adsorbed. The $MgCl_2$ contains only Mg^{2+} cations, but the inlet position is also the position where calcite dissolves fastest and magnesite precipitates fastest. Because of that a balance develops and so the surface is dominated, but not completely filled, by Mg^{2+}.

Also, since the solution gains Ca^{2+} and loses Mg^{2+} along the core we see that accordingly the surface contains more Ca^{2+} further into the core and thus less Mg^{2+}. Since the two β s are really dependent as $\beta_{ca}+\beta_{mg}=1$ for this system the second plot simply shows the opposite trend for Mg^{2+} as for Ca^{2+}. The composition distributions reach a steady state after 3 days. This is a natural consequence of its dependence on the brine composition which then also has reached a steady state.

Mineral distribution

The resulting changes in mineral content by the flooding are seen in Fig. 14. The plot for calcite shows that the initial distribution is uniform with nonzero concentration. As flooding begins the calcite concentration reduces due to dissolution, but the effect is best seen at the inlet. Similarly in the plot for magnesite a zero initial concentration increases due to mineral precipitation and most at the inlet.

Unlike the distributions for ions in solution and on surface, the mineral composition does not approach a steady state. Rather, after the ion concentration distributions have reached a steady state it seems the mineral concentrations change as much as ever. In effect, at a given point the mineral concentration changes linearly in time, which can be seen both for calcite and magnesite.

From the predicted and experimental effluent we have confirmed that for $MgCl_2$ the sum of Ca^{2+} and Mg^{2+} concentrations equal the injected Mg^{2+}, meaning that on average any produced Ca^{2+}-ion is replaced by a Mg^{2+}-ion. The plots also indicate that the local precipitation of magnesite closely compensates for the dissolution of calcite so that the changes in porosity even locally are

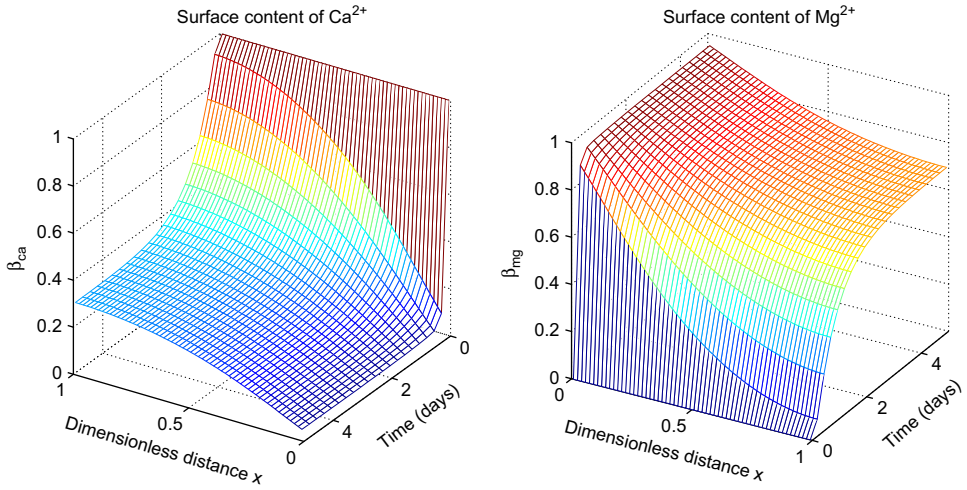

Fig. 13. 3D visualization of the surface ion distribution in time for 0.109 M $MgCl_2$.

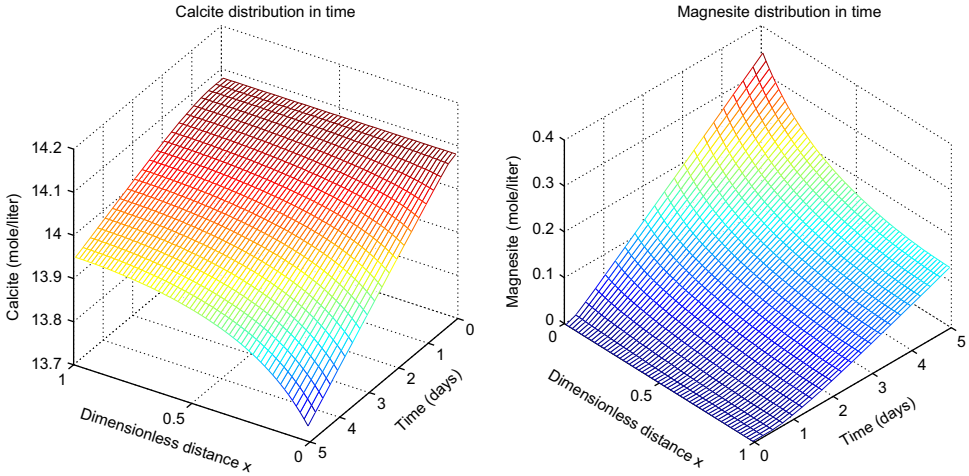

Fig. 14. 3D visualization of the mineral distribution in time for 0.109 M $MgCl_2$.

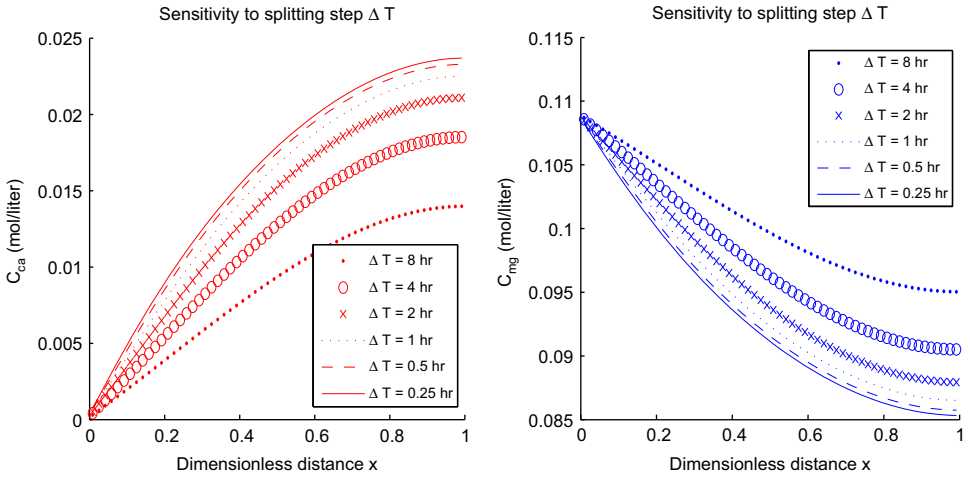

Fig. 15. Sensitivity to splitting step by comparing ion distribution after 5 days flooding of 0.109 M $MgCl_2$.

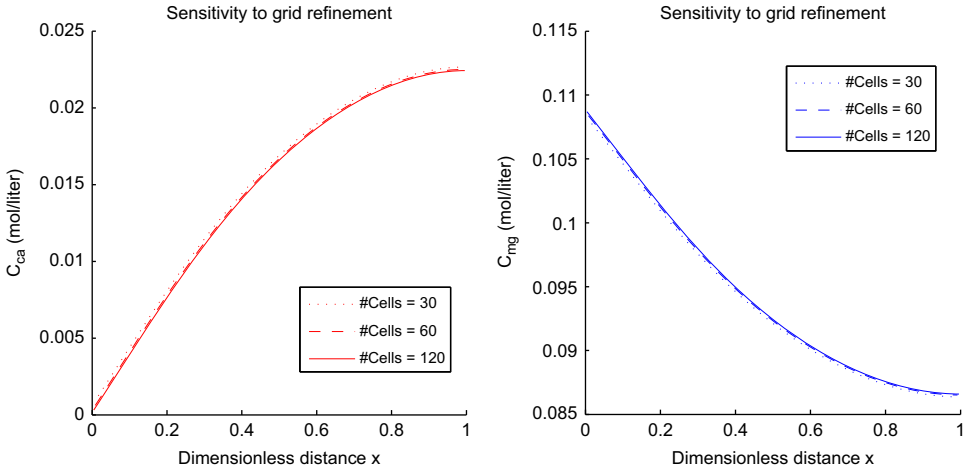

Fig. 16. Sensitivity to grid refinement by comparing ion distribution after 5 days flooding of 0.109 M $MgCl_2$.

not very dramatic. This of course only describes the changes by mass transfer in a constant volume system, there are also changes due to compression of the core in the experimental setting.

4.6. Test of numerical convergence

To demonstrate the accuracy of the produced solutions a refinement of the grid and the splitting time step has been performed. We still consider 0.109 M $MgCl_2$ with initial Ca^{2+} on the surface 0.15 (mol/l). The base case is $\Delta t = 1$ h and 60 cells, with runtime 5 days.

Fig. 15 shows the effect of varying the splitting step by factors of 2 compared to the standard of 1 h, while using 60 cells. For illustration the ion distributions of Ca^{2+} and Mg^{2+} have been used. It is seen that as the time of the splitting step goes towards 0 the solutions do not differ very much, i. e. the solutions converge. Our chosen value for the splitting step produces solutions reasonably close to this limit.

To see the effect of the number of grid cells we also here used a factor of 2 compared to the standard, which was 60 cells, while the splitting step was constant 1 h. As seen in Fig. 16 there is little variation, even between the cases with 30 and 120 cells.

5. Concluding remarks

The main contribution of this work is that we extend the model previously developed in Evje et al. (2009) and Madland et al. (2011) for interpretation of various laboratory flooding experiments in the context of chalk water-weakening studies. The first version of the model focused on the combined effect of transport and water–rock chemistry in terms of dissolution/precipitation. The new aspect of this work is that we include in the full transient model some important complexes, whose selection is based on PHREEQC equilibrium calculations, as well as ion exchange processes relevant for the flooding experiments. We then demonstrate how the model is able to capture the early transient behavior observed in the effluent concentrations as well as the steady state behavior. It is the combined effect of ion exchange and dissolution/precipitation that gives the most interesting behavior when compared to the experimental data. We demonstrate that the proposed model seems to be a promising tool for describing water–rock chemistry relevant for flooding experiments with chalk. However, one should keep in mind that the model is designed for a special setting. It is not a general geochemical simulator as it is closely linked to the special system that has been studied in the laboratory. The model can work as a

history-matching tool and it is possible to vary which mechanisms to focus on. Seven parameters have been determined in this work: dispersivity α; cation exchange capacity CEC; cation exchange constants $K_{na/ca}$ and $K_{na/mg}$; and three reaction rate parameters: k_c, k_g, k_m. A description has been provided to determine the parameters one by one.

We include several chemical mechanisms. However, we treat them in a simplified manner to see their main effects, while minimizing the amount of complex couplings and use of computational resources. Ionic strength, activity coefficients, temperature, porosity, P_{co2}, complexation fractioning are all treated as constants during a simulation, but such that we include the dependence on brine, temperature and ion.

The main agents on the chalk surface appear to be Ca^{2+} and Mg^{2+} as seen in these experiments. Results indicate that Na^+ interacts weakly with the chalk surface, partly because of its high relative concentration in the considered brines. The SO_4^{2-} effluent is mostly explained in terms of anhydrite precipitation although surface interaction might also play a role.

The results for flooding with NaCl, $MgCl_2$ and seawater-like brines of ionic strength between 0.3 and 0.7 and pH between 6.0 and 8.5 are explained well with the model. Different possible sources for inaccuracies might be:

- The kinetics are not fully understood and it is of interest to make use of SEM results for an improved description, see also Remark 4.
- There could be more minerals involved, and they could form as non-pure phases. Clays can act as exchanger and explain the apparent Na^+ adsorption. Sulfate adsorption can play an important role, but this should be matched with experiments where it is dominant.
- Different parameters may depend on the experimental conditions or change during the experiment instead of being constants.

To further reduce the discrepancies between the observed and modeled data it is possible to include some of the above listed effects in a continuously updated model. By that we mean to update ionic strength, activity coefficients, free ion and complex concentrations, include the carbon chemistry in full detail (and not use the P_{co2} concept) and let porosity change with the mineral concentrations. We can also add more parameters to fit the experimental data. We have used fixed rate coefficients, dispersion coefficient/dispersivity and CEC. The transient effluent can be better approximated using a rate dependent ion exchange where we also allow a brine-dependent rate coefficient. The effluent seems to change linearly with time after the peak has been reached. Dissolution/precipitation become more dominant and the precipitation of the new minerals could reduce the CEC by covering the surface. Or perhaps the dissolution of calcite exposes more reactive sites? In this sense we could have a relation between the local CEC and the mineral concentrations.

Finally, we would like to emphasize that although focus has been on experiments performed at 130 °C the model can be applied to other temperatures as equilibrium constants are available in the literature and the given rate constants can be taken as a starting point. Since we expect these coefficients to be temperature dependent history matching at other temperatures can provide an estimate of this correlation.

Acknowledgments

This research has been supported by A/S Norske Shell.

Appendix A

A.1. Ion exchange calculations

The following system must be solved and we are especially interested in ρ_{ca},ρ_{mg},ρ_{na}:

$$K_{na/ca} = \frac{\beta_{na}}{\beta_{ca}^{0.5}} \frac{\gamma_{ca}^{0.5} m_{ca}^{0.5}}{\gamma_{na} m_{na}},$$

$$K_{na/mg} = \frac{\beta_{na}}{\beta_{mg}^{0.5}} \frac{\gamma_{mg}^{0.5} m_{mg}^{0.5}}{\gamma_{na} m_{na}},$$

$$\beta_{ca} + \beta_{mg} + \beta_{na} = 1,$$

$$\rho_{ca}^s + \rho_{ca} = \rho_{ca}^{tot},$$

$$\rho_{mg}^s + \rho_{mg} = \rho_{mg}^{tot},$$

$$\rho_{na}^s + \rho_{na} = \rho_{na}^{tot},$$

$$\rho_{ca}^s \cdot 2 = \beta_{ca} \cdot CEC,$$

$$\rho_{mg}^s \cdot 2 = \beta_{mg} \cdot CEC,$$

$$\rho_{na}^s \cdot 1 = \beta_{na} \cdot CEC,$$

$$m_{ca} = r_{ca}\rho_{ca}/\phi,$$

$$m_{mg} = r_{mg}\rho_{mg}/\phi,$$

$$m_{na} = r_{na}\rho_{na}/\phi. \tag{A.1}$$

Combining the last six equations with the first six gives

$$K_{na/ca} = \frac{\beta_{na}}{\beta_{ca}^{0.5}} \frac{(\gamma_{ca} r_{ca} \rho_{ca}/\phi)^{0.5}}{\gamma_{na} r_{na} \rho_{na}/\phi} = \frac{\beta_{na}}{\beta_{ca}^{0.5}} \frac{\rho_{ca}^{0.5}}{\rho_{na}} \frac{(\gamma_{ca} r_{ca} \phi)^{0.5}}{\gamma_{na} r_{na}},$$

$$K_{na/mg} = \frac{\beta_{na}}{\beta_{mg}^{0.5}} \frac{(\gamma_{mg} r_{mg} \rho_{mg}/\phi)^{0.5}}{\gamma_{na} r_{na} \rho_{na}/\phi} = \frac{\beta_{na}}{\beta_{mg}^{0.5}} \frac{\rho_{mg}^{0.5}}{\rho_{na}} \frac{(\gamma_{mg} r_{mg} \phi)^{0.5}}{\gamma_{na} r_{na}},$$

$$\beta_{ca} + \beta_{mg} + \beta_{na} = 1,$$

$$\beta_{ca} \cdot CEC/2 + \rho_{ca} = \rho_{ca}^{tot},$$

$$\beta_{mg} \cdot CEC/2 + \rho_{mg} = \rho_{mg}^{tot},$$

$$\beta_{na} \cdot CEC + \rho_{na} = \rho_{na}^{tot}. \tag{A.2}$$

We now choose to express the system only by ρ's. Tilde constants are defined to collect various constants into one single constant. Hence, by algebraic manipulations we get from (A.2)

$$\frac{\beta_{na}}{\beta_{ca}^{0.5}} \frac{\rho_{ca}^{0.5}}{\rho_{na}} = \tilde{K}_{na/ca} := K_{na/ca} \frac{\gamma_{na} r_{na}}{(\gamma_{ca} r_{ca} \phi)^{0.5}},$$

$$\frac{\beta_{na}}{\beta_{mg}^{0.5}} \frac{\rho_{mg}^{0.5}}{\rho_{na}} = \tilde{K}_{na/mg} := K_{na/mg} \frac{\gamma_{na} r_{na}}{(\gamma_{mg} r_{mg} \phi)^{0.5}},$$

$$\beta_{ca} + \beta_{mg} + \beta_{na} = 1,$$

$$\beta_{ca} = 2(\rho_{ca}^{tot} - \rho_{ca})/CEC,$$

$$\beta_{mg} = 2(\rho_{mg}^{tot} - \rho_{mg})/CEC,$$

$$\beta_{na} = (\rho_{na}^{tot} - \rho_{na})/CEC. \tag{A.3}$$

The β's are substituted into the first three equations of (A.3) and we get

$$\frac{(\rho_{na}^{tot}-\rho_{na})/CEC}{(2(\rho_{ca}^{tot}-\rho_{ca})/CEC)^{0.5}}\frac{\rho_{ca}^{0.5}}{\rho_{na}}=\tilde{K}_{na/ca},$$

$$\frac{(\rho_{na}^{tot}-\rho_{na})/CEC}{(2(\rho_{mg}^{tot}-\rho_{mg})/CEC)^{0.5}}\frac{\rho_{mg}^{0.5}}{\rho_{na}}=\tilde{K}_{na/mg},$$

$$2(\rho_{ca}^{tot}-\rho_{ca})/CEC+2(\rho_{mg}^{tot}-\rho_{mg})/CEC+(\rho_{na}^{tot}-\rho_{na})/CEC=1, \tag{A.4}$$

and concentrations are expressed by ρ_{ca} as follows:

$$\rho_{na}=\frac{\rho_{na}^{tot}}{\sqrt{2\tilde{K}_{na/ca}^2 CEC\left(\frac{\rho_{ca}^{tot}}{\rho_{ca}}-1\right)}+1},$$

$$\rho_{mg}=\frac{\rho_{mg}^{tot}}{\frac{1}{2\tilde{K}_{na/mg}^2 CEC}\left(\frac{\rho_{na}^{tot}}{\rho_{na}}-1\right)^2+1}=\frac{\rho_{mg}^{tot}}{\frac{\tilde{K}_{na/ca}^2}{\tilde{K}_{na/mg}^2}\left(\frac{\rho_{ca}^{tot}}{\rho_{ca}}-1\right)+1},$$

$$2\rho_{ca}+2\frac{\rho_{mg}^{tot}}{\frac{\tilde{K}_{na/ca}^2}{\tilde{K}_{na/mg}^2}\left(\frac{\rho_{ca}^{tot}}{\rho_{ca}}-1\right)+1}+\frac{\rho_{na}^{tot}}{\sqrt{2\tilde{K}_{na/ca}^2 CEC\left(\frac{\rho_{ca}^{tot}}{\rho_{ca}}-1\right)}+1}$$
$$=(2\rho_{ca}^{tot}+2\rho_{mg}^{tot}+\rho_{na}^{tot})-CEC:=SEC. \tag{A.5}$$

Note that we have defined the current *solution equivalents content* as *SEC*. The last equation of (A.5) must be solved for ρ_{ca}.

$$\rho_{ca}=\frac{1}{2}\left(-2\frac{\rho_{mg}^{tot}}{\frac{\tilde{K}_{na/ca}^2}{\tilde{K}_{na/mg}^2}\left(\frac{\rho_{ca}^{tot}}{\rho_{ca}}-1\right)+1}-\frac{\rho_{na}^{tot}}{\sqrt{2\tilde{K}_{na/ca}^2 CEC\left(\frac{\rho_{ca}^{tot}}{\rho_{ca}}-1\right)}+1}+SEC\right). \tag{A.6}$$

Divide by ρ_{ca}^{tot} and set $x\equiv\rho_{ca}/\rho_{ca}^{tot}$. It follows that $0\le x\le 1$. Moreover, (A.6) gives the following nonlinear algebraic equations in terms of x.

$$x=f(x)=\frac{1}{2}\left(-2\frac{\rho_{mg}^{tot}/\rho_{ca}^{tot}}{\frac{\tilde{K}_{na/ca}^2}{\tilde{K}_{na/mg}^2}\left(\frac{1}{x}-1\right)+1}-\frac{\rho_{na}^{tot}/\rho_{ca}^{tot}}{\sqrt{2\tilde{K}_{na/ca}^2 CEC\left(\frac{1}{x}-1\right)}+1}+SEC/\rho_{ca}^{tot}\right). \tag{A.7}$$

Considering the endpoints of this function we have at $x=0$

$$f(0)=\frac{1}{2}(SEC/\rho_{ca}^{tot})\ge 0$$

and at $x=1$

$$f(1)=\frac{1}{2}(-2\rho_{mg}^{tot}/\rho_{ca}^{tot}-\rho_{na}^{tot}/\rho_{ca}^{tot}+SEC/\rho_{ca}^{tot})=1-\frac{1}{2}CEC/\rho_{Ca}^{tot}\le 1.$$

The function $f(x)-x$ is monotonously decreasing relatively x on [0, 1]. Since $f(0)-0>0$ and $f(1)-1<0$ there exists a unique solution which solves the entire set of equations. A solution can be found by the bisection method with limits $f_{max}=f(0)$ and $f_{min}=f(1)$.

To sum up: Knowing the total concentrations ρ_i^{tot} defined by (A.1) (fourth, fifth, and sixth equation) and CEC for the rock we consider, we can calculate ρ_{ca} first by solving for x satisfying (A.7). Then, we can calculate the other brine concentrations ρ_{na} and ρ_{mg} from the two first equations of (A.5). Finally, we can obtain the corresponding concentrations ρ_{ca}^s, ρ_{mg}^s, and ρ_{na}^s representing ions attached to the rock, and then also the fractions β_i, $i=ca, mg, na$, see (A.1).

A.2. The electroneutrality condition

The following aqueous charge balance equation is assumed to hold for the various species contained in the water phase

$$\sum_i^{N_b} m_i Z_i+\sum_i^{N_c} n_i Z_i=0. \tag{A.8}$$

For the system in question, this results in the following balance equation:

$$2m_{ca}+2m_{mg}+m_h+m_{na}+n_{mgcl}+n_{cacl}=2m_{so}+m_{hco}+2m_{co}+m_{oh}+m_{cl}+n_{naso}. \tag{A.9}$$

In particular, we can solve for m_h, m_{hco}, m_{co}, and m_{oh}. To see the details, first, we note that (A.9) can be written in the form

$$M=m_{hco}+2m_{co}+m_{oh}-m_h, \tag{A.10}$$

where

$$\begin{aligned}M&=2(m_{ca}+m_{mg}-m_{so})+(m_{na}-m_{cl})-n_{naso}+n_{cacl}+n_{mgcl}\\&=2(C_{ca}+C_{mg}-C_{so})+(C_{na}-C_{cl})\\&=:M(C_{ca},C_{mg},C_{so};C_{na},C_{cl}),\end{aligned} \tag{A.11}$$

where we have used (5). Note that the calculation described below and based on M, implies that both complexes and ion exchange have been decoupled. The reason for this is that the amount of equivalents in M is the same no matter how it is distributed between free ions and complexes, and also because any charge transfer between solution and surface is instantly maintained.

It is convenient to introduce the following notation:

$$\tilde{K}_{co}=\frac{K_{co}}{\gamma_{hco}\gamma_h},\quad \tilde{K}_{hco}=\frac{K_{hco}\gamma_{hco}}{\gamma_{co}\gamma_h},\quad \tilde{K}_w=\frac{K_w}{\gamma_h\gamma_{oh}}. \tag{A.12}$$

We shall make use of the simplifying assumption that the concentration m_{co} of CO_3^{2-} is relatively low for a pH in the range [6,8] and can be neglected in the charge balance equation (A.10). Clearly, (A.10) can then be written in the form

$$M=m_{hco}+\frac{\tilde{K}_w}{m_h}-m_h, \tag{A.13}$$

where we have used (15). Combining (12) and (20), (A.12), and (A.13) we get

$$M=\frac{\tilde{K}_{co}+\tilde{K}_w}{m_h}-m_h,$$

which results in the second order equation $m_h^2+Mm_h-(\tilde{K}_{co}+\tilde{K}_w)=0$. The relevant solution is then given by

$$m_h=\frac{1}{2}(-M+\sqrt{M^2+4(\tilde{K}_{co}+\tilde{K}_w)}),\quad m_{hco}=\frac{\tilde{K}_{co}}{m_h}. \tag{A.14}$$

Finally, m_{co} and m_{oh} can be determined from (14) and (15). In particular, we note that $m_h=m_h(C_{ca},C_{so},C_{mg};C_{na},C_{cl})$, in view of (A.11). Thus, the calculation of pH has been decoupled from ion exchange and complexes.

Appendix B. Numerical discretization

For the numerical method that is used to solve the system of convection–diffusion–reaction equations (73)–(76), we refer to Evje et al. (2009), Yu et al. (2008), Faugeras et al. (2005), LeVeque (2002), and Steefel and Lasaga (1994) for relevant information. We here briefly recall the main steps. Let us introduce

$$\mathbf{C}=(\phi C_{na},\phi C_{cl},\phi C_{ca},\phi C_{so},\phi C_{mg})^T,\quad \mathbf{S}=(\rho_{na}^s,0,\rho_{ca}^s,0,\rho_{mg}^s,)^T,$$
$$\mathbf{U}=(\rho_c,\rho_g,\rho_m)^T.$$

We assume that we have approximate solutions $([\mathbf{C}+\mathbf{S}]^n(\cdot),\mathbf{U}^n(\cdot))\approx([\mathbf{C}+\mathbf{S}](\cdot,t^n),\mathbf{U}(\cdot,t^n))$. Now, we want to calculate an

approximation at the next time level $([\mathbf{C}+\mathbf{S}]^{n+1}(\cdot),\mathbf{U}^{n+1}(\cdot)) \approx ([\mathbf{C}+\mathbf{S}](\cdot,t^{n+1}),\mathbf{U}(\cdot,t^{n+1}))$ by using a three-step operator splitting approach. More precisely, the idea we implement is to treat in separate steps transport of ions in solution, chemical reaction in terms of dissolution and precipitation, and ion exchange. For that purpose we introduce the operators T_t, D_t, and F_0 as follows:

B.1. Operator D_t: dissolution and precipitation

Let D_t be the operator associated with the precipitation and dissolution reaction part of (73), i.e. D_t represents the solution of the following system of ODEs for a local time interval $t \in [0,\Delta t]$:

$$\frac{d(\phi C_{na}+\rho^s_{na})}{dt}=0,$$

$$\frac{d(\phi C_{cl})}{dt}=0,$$

$$\frac{d(\phi C_{ca}+\rho^s_{ca})}{dt}=A^c[\mathrm{sgn}^+(\rho_c)(F_c^+)^{n_c}-(F_c^-)^{n_c}]+A^g[\mathrm{sgn}^+(\rho_g)(F_g^+)^{n_g}-(F_g^-)^{n_g}],$$

$$\frac{d(\phi C_{so})}{dt}=A^g[\mathrm{sgn}^+(\rho_g)(F_g^+)^{n_g}-(F_g^-)^{n_g}],$$

$$\frac{d(\phi C_{mg}+\rho^s_{mg})}{dt}=A^m[\mathrm{sgn}^+(\rho_m)(F_m^+)^{n_m}-(F_m^-)^{n_m}],$$

$$\frac{d\rho_c}{dt}=-A^c[\mathrm{sgn}^+(\rho_c)(F_c^+)^{n_c}-(F_c^-)^{n_c}],$$

$$\frac{d\rho_g}{dt}=-A^g[\mathrm{sgn}^+(\rho_g)(F_g^+)^{n_g}-(F_g^-)^{n_g}],$$

$$\frac{d\rho_m}{dt}=-A^m[\mathrm{sgn}^+(\rho_m)(F_m^+)^{n_m}-(F_m^-)^{n_m}], \tag{B.1}$$

where $A^I=\tau\phi k^I$, for $I=c, g, m$. Here F_I are given by (39). We keep the surface concentration ρ_i^s of the various species $i=na, ca, mg$ constant since we solve for this in a separate step. Hence, the concentrations C_{na} and C_{cl} also remain unaltered during this step. As a consequence, the system (B.1) corresponds to solving for $t \in [0,\Delta t]$

$$C_{na}(t)=C_{na}(t=0),\quad C_{cl}(t)=C_{cl}(t=0),$$

$$\rho^s_{na}(t)=\rho^s_{na}(t=0),\quad \rho^s_{ca}(t)=\rho^s_{ca}(t=0),\qquad \rho^s_{mg}(t)=\rho^s_{mg}(t=0),$$

$$\frac{dC_{ca}}{dt}=\frac{A^c}{\phi}[\mathrm{sgn}^+(\rho_c)F_c^+(C_{ca},C_{so},C_{mg})-F_c^-(C_{ca},C_{so},C_{mg})]+\frac{A^g}{\phi}[\mathrm{sgn}^+(\rho_g)F_g^+(C_{ca},C_{so},C_{mg})-F_g^-(C_{ca},C_{so},C_{mg})],$$

$$\frac{dC_{so}}{dt}=\frac{A^g}{\phi}[\mathrm{sgn}^+(\rho_g)F_g^+(C_{ca},C_{so},C_{mg})-F_g^-(C_{ca},C_{so},C_{mg})],$$

$$\frac{dC_{mg}}{dt}=\frac{A^m}{\phi}[\mathrm{sgn}^+(\rho_m)F_m^+(C_{ca},C_{so},C_{mg})-F_m^-(C_{ca},C_{so},C_{mg})], \tag{B.2}$$

where

$$\rho_c(t)=\rho_{c,0}-\phi(C_{ca}-C_{so})(t)+\phi(C_{ca,0}-C_{so,0}),$$

$$\rho_g(t)=\rho_{g,0}-\phi(C_{so}(t)-C_{so,0}),$$

$$\rho_m(t)=\rho_{m,0}-\phi(C_{mg}(t)-C_{mg,0}), \tag{B.3}$$

which is obtained by combining the six last equations of (B.1). Hence, we obtain an updated approximate solution of (73) in terms of total concentrations

$$([\mathbf{C}+\mathbf{S}],\mathbf{U})(\cdot,\Delta t)=(\tilde{\mathbf{C}}(\cdot,\Delta t)+\mathbf{S}(\cdot,0),\mathbf{U}(\cdot,\Delta t)),$$

where $(\tilde{\mathbf{C}},\mathbf{U})$ is the solution of (B.2) and (B.3) and the tilde-notation is used to indicate that ion-exchange has not been taken into account.

Thus, we obtain intermediate approximations $([\mathbf{C}+\mathbf{S}]^{n+1/2},\mathbf{U}^{n+1/2})=D_{\Delta t}(\mathbf{C}^n,\mathbf{S}^n,\mathbf{U}^n)$. The stiff ODE system given by (B.2) and (B.3) is solved by using the Matlab function ode23 (Evje et al., 2009).

B.2. Operator T_t: advection and diffusion

Let T_t be the operator associated with the solution of the transport part of (73), i.e. T_t represents the solution of the following system of parabolic PDEs:

$$\partial_t(\phi C_{na}+\rho^s_{na})+\partial_x(C_{na}J)=\partial_x(D\phi\partial_x C_{na}),$$

$$\partial_t(\phi C_{cl})+\partial_x(C_{cl}J)=\partial_x(D\phi\partial_x C_{cl}),$$

$$\partial_t(\phi C_{ca}+\rho^s_{ca})+\partial_x(C_{ca}J)=\partial_x(D\phi\partial_x C_{ca}),$$

$$\partial_t(\phi C_{so})+\partial_x(C_{so}J)=\partial_x(D\phi\partial_x C_{so}),$$

$$\partial_t(\phi C_{mg}+\rho^s_{mg})+\partial_s(C_{mg}J)=\partial_x(D\phi\partial_x C_{mg}),$$

$$\partial_t\rho_c=\partial_t\rho_g=\partial_t\rho_m=0. \tag{B.4}$$

As for the dissolution/precipitation operator D_t, we do not account for changes in the surface concentrations ρ_i^s in this step since this is treated in a separate step. Hence, we obtain an updated approximate solution of (73) in terms of total concentrations

$$([\mathbf{C}+\mathbf{S}],\mathbf{U})(\cdot,\Delta t)=(\tilde{\mathbf{C}}(\cdot,\Delta t)+\mathbf{S}(\cdot,0),\mathbf{U}(\cdot,0)),$$

where $\tilde{\mathbf{C}}$ is the solution of (B.5) given by

$$\partial_t(\phi C_{na})+\partial_x(C_{na}J)=\partial_x(D\phi\partial_x C_{na}),$$

$$\partial_t(\phi C_{cl})+\partial_x(C_{cl}J)=\partial_x(D\phi\partial_x C_{cl}),$$

$$\partial_t(\phi C_{ca})+\partial_x(C_{ca}J)=\partial_x(D\phi\partial_x C_{ca}),$$

$$\partial_t(\phi C_{so})+\partial_x(C_{so}J)=\partial_x(D\phi\partial_x C_{so}),$$

$$\partial_t(\phi C_{mg})+\partial_s(C_{mg}J)=\partial_x(D\phi\partial_x C_{mg}), \tag{B.5}$$

and the tilde-notation is used to indicate that ion-exchange has not been taken into account. From this we find $([\mathbf{C}+\mathbf{S}]^{n+1},\mathbf{U}^{n+1})=T_{\Delta t}(\mathbf{C}^{n+1/2},\mathbf{S}^{n+1/2},\mathbf{U}^{n+1/2})$.

B.3. Operator F_0: ion exchange

We also need to take into account in an appropriate manner the ion exchange reactions coupled with the PDE system. Considering the system without transport and precipitation/dissolution reactions we have

$$\partial_t(\phi C_{na}+\rho^s_{na})=0,$$

$$\partial_t(\phi C_{cl})=0,$$

$$\partial_t(\phi C_{ca}+\rho^s_{ca})=0,$$

$$\partial_t(\phi C_{so})=0,$$

$$\partial_t(\phi C_{mg}+\rho^s_{mg})=0,$$

$$\partial_t\rho_c=\partial_t\rho_g=\partial_t\rho_m=0. \tag{B.6}$$

The starting point is that we know the total concentrations $\mathbf{C}+\mathbf{S}$, let us say at time t^n, that is, $([\mathbf{C}+\mathbf{S}]^n,\mathbf{U}^n)$ produced by applying the operators D_t or T_t as described above. According to (B.6), the purpose of the ion exchange operator F_0 is then to find the

redistribution represented by the solution $(\mathbf{C}^n,\mathbf{S}^n,\mathbf{U}^n)$, where

$$(\mathbf{C}^n,\mathbf{S}^n)=F_0[\mathbf{C}+\mathbf{S}]^n,$$

and the detailed calculation represented by F_0 is as outlined in Section 2.4, and such that

$$\mathbf{C}^n+\mathbf{S}^n=[\mathbf{C}+\mathbf{S}]^n.$$

Hence, the application of this step is to redistribute the cations between surface and brine to be in equilibrium. The application of the ion exchange operator F_0 is made before every reaction or transport step.

B.4. The operator splitting method

The numerical method that is used to solve the system (73) is based on a proper combination of the various operators D_t, T_t, and F_0 described above, and represents a natural extension of the approach used for the model without ion exchange (Evje et al., 2009; Yu et al., 2008). More precisely, the following Strang type of splitting (Faugeras et al., 2005; Strang, 1968) is employed:

$$([\mathbf{C}+\mathbf{S}]^{n+1},\mathbf{U}^{n+1})=[T_{\Delta t/2}F_0D_{\Delta t}F_0T_{\Delta t/2}F_0]([\mathbf{C}+\mathbf{S}]^n,\mathbf{U}^n). \quad (B.7)$$

Hence, before every step of reaction D_t or transport T_t the system is equilibrated with respect to ion exchange F_0. In other words, for every splitting time step Δt, ion exchange calculations have been performed three times.

Appendix C

C.1. Mineral properties

Molar weights M_i and densities ω_i of calcite (c), anhydrite (g) and magnesite (m).

$$M_c=100.087\ \text{g/mol},\quad M_g=136.139\ \text{g/mol}\quad M_m=84.314\ \text{g/mol},$$

$$\omega_c=2710\ \text{g/l},\quad \omega_g=2970\ \text{g/l},\quad \omega_m=3100\ \text{g/l}. \quad (C.1)$$

C.2. Thermodynamic data

Ion specific parameters a_i,b_i collected from Appelo and Postma (2009) and Lasaga (1998) for calculation of activity coefficients by Truesdell Jones formula (7) are given in Table C1.

Values for $A(T)$ and $B(T)$ at surface (25 °C) and experimental (130 °C) conditions

$$A(T=25)=0.5085,\quad B(T=25)=0.3285,$$

$$A(T=130)=0.6623,\quad B(T=130)=0.3487. \quad (C.2)$$

These values are taken from Appelo and Postma (2009) and the EQAlt-simulator (Hiorth et al., 2008).

Table C1
Constants to be used in Truesdell Jones formula (7).

i	a_i	b_i
h	4.78	0.24
oh	10.65	0.21
co	5.4	0
ca	5	0.165
hco	5.4	0
na	4	0.075
cl	3.5	0.015
mg	5.5	0.20
so	5	−0.04

C.3. Equilibrium constants and solubility products

Table C2 contains solubility products for mineral reactions (1) and equilibrium constants for reactions (2), (3), and (4) at both surface and experimental temperatures (25 and 130 °C).

C.4. Brine compositions

Brine compositions defined by fluid concentrations C in (mol/l) are given in Table C3.

Table C2
Thermodynamic constants.

	$T=25$	$T=130$		$T=25$	$T=130$
K^c	$10^{+1.86}$	$10^{+0.35}$	K_{caso}	$10^{-2.30}$	$10^{-2.78}$
K^g	$10^{-4.3}$	$10^{-5.94}$	K_{naso}	$10^{-0.70}$	$10^{-1.27}$
K^m	$10^{+2.3}$	$10^{-0.01}$	K_{mgso}	$10^{-2.37}$	$10^{-2.90}$
K	$10^{-7.87}$	$10^{-9.01}$	K_{cacl}	$10^{+0.67}$	$10^{+0.15}$
K_{co2}	$10^{-6.39}$	$10^{-6.98}$	K_{mgcl}	$10^{+0.11}$	$10^{-0.40}$
K_{hco}	$10^{-10.32}$	$10^{-10.15}$	$K^{soil}_{na/ca}$	$10^{-0.40}$	$10^{-0.07}$
K_w	$10^{-14.05}$	$10^{-12.26}$	$K^{soil}_{na/mg}$	$10^{-0.30}$	$10^{+0.04}$

Table C3
Composition of the different brines.

Ions	$MgCl_2$-I (mol/l)	$MgCl_2$-II (mol/l)	NaCl (mol/l)	SSW-I (mol/l)	SSW-II (mol/l)	Na_2SO_4 (mol/l)
Na^+	0.000	0.000	0.657	0.4501	0.0500	0.438
Cl^-	0.218	0.438	0.657	0.5252	0.1251	0.000
Ca^{2+}	0.000	0.000	0.000	0.0130	0.0130	0.000
Mg^{2+}	0.109	0.219	0.000	0.0240	0.0240	0.000
SO_4^{2-}	0.000	0.000	0.000	0.0445	0.0445	0.219
K^+	0.000	0.000	0.000	0.0101	0.0101	0.000
Ion strength I_0 from (9)	0.327	0.657	0.657	0.656	0.256	0.657

Table D1
List of designations.

ρ_i	Species concentration (mol/l rock)	ϕ	Porosity (–)
C_i	Species concentration (mol/l fluid)	a_i	Activity (–)
ρ_i^s	Surface species concentration (mol/l rock)	γ_i	Activity coefficient (–)
m_i	Uncomplexed species concentration (mol/l fluid)	I_0	Ionic strength (–)
n_i	Complexed species concentration (mol/l fluid)	Z_i	Charge valence (–)
A,B	Temperature dependent parameters	K_i	Equilibrium constants
a_i,b_i	Ion specific parameters	TIC	Total inorganic carbon
P_{co2}	Partial pressure of CO_2 (bar)	Ω	Saturation index
r_i	Fraction of uncomplexed species (–)	ω	Mineral density (g/l)
CEC	Cation exchange capacity (eq/l rock)	κ	Permeability (m^2)
M_i	Mineral molar weight (g/mol)	ν	Viscosity (Pa s)
β_i	Surface cation equivalent fraction (–)	p	Pressure (Pa)
SEC	Solution cation equivalents content (eq/l rock)	L	Core length (m)
M	Equivalents of main species (eq/l fluid)	τ	Time scale (s)
k_i	Reaction rate constant (mol/l rock/s)	q	Injection rate (PV/d)
n_i	Exponential rate factor (–)	Δt	Splitting step
D	Dispersion coefficient (m^2/s)		
D_m	Molecular diffusion coefficient (m^2/s)		
α	Dispersivity (m)		
V	Seepage velocity (m/s)		
C	Water concentration (mol/l fluid)		
J	Dimensionless seepage velocity (–)		

Appendix D. List of designations

The list of designations are given in Table D1.

References

Ali, G., Furuholt, V., Natalini, R., Torcicollo, I., 2007a. A mathematical model of sulphite chemical aggression of limestones with high permeability. Part I. Modeling and qualitative analysis. Transp. Porous Media 69, 109–122.

Ali, G., Furuholt, V., Natalini, R., Torcicollo, I., 2007b. A mathematical model of sulphite chemical aggression of limestones with high permeability. Part II. Numerical approximation. Transp. Porous Media 69, 175–188.

Appelo, C.A.J., Postma, D., 2009. Geochemistry, Groundwater and Pollution. Taylor & Francis Group.

Aregba-Driollet, D., Diele, F., Natalini, R., 2004. A mathematical model for the sulphur dioxide aggression to calcium carbonate stones: numerical approximation and asymptotic analysis. SIAM J. Appl. Math. 64 (5), 1636–1667.

Austad, T., Standnes, D.C., 2003. Wettability and oil recovery from carbonates: effects of temperature and potential determining ions. J. Pet. Sci. Eng. 39, 363–376.

Bouillard, N., Eymard, R., Herin, R., Montarnal, P., 2007. Diffusion with dissolution and precipitation in a porous medium: mathematical analysis and numerical approximation of a simplified model. ESAIM: M2AN 41 (6), 975–1000.

Bouillard, N., Eymard, R., Herbin, R., Montarnal, P., 2009. A fast precipitation and dissolution reaction for a reaction–diffusion system arising in a porous medium. Nonlinear Anal. Real World Appl. 10, 629–638.

van Duijn, C.J., Knabner, P., Schotting, R.J., 1998. An analysis of crystal dissolution fronts in flows through porous media. Part 2: incompatible boundary conditions. Adv. Water Resour. 22 (1), 1–16.

van Duijn, C.J., Knabner, P., 1992a. Travelling waves in the transport of reactive solutes through porous media: adsorption and binary ion exchange. Part 1. Transp. Porous Media 8, 167–194.

van Duijn, C.J., Knabner, P., 1992b. Travelling waves in the transport of reactive solutes through porous media: adsorption and binary ion exchange. Part 2. Transp. Porous Media 8, 199–225.

Engesgaard, P., Kipp, K.L., 1992. A geochemical transport model for redox-controlled movement of mineral fronts in groundwater flow systems: a case of nitrate removal by oxidation of pyrite. Water Resour. Res. 28 (10), 2829–2843.

Evje, S., Hiorth, A., Madland, M.V., Korsnes, R., 2009. A mathematical model relevant for weakening of chalk reservoirs due to chemical reactions. Networks Heterogeneous Media 4 (4), 755–788.

Evje, S., Hiorth, A., 2010. A mathematical model for dynamic wettability alteration controlled by water–rock chemistry. Networks Heterogeneous Media 5 (2), 217–256.

Evje, S., Hiorth, A., 2011. A model for interpretation of brine-dependent spontaneous imbibition experiments. Adv. Water Resour. 34 (12), 1627–1642.

Faugeras, B., Pousin, J., Fontvieille, F., 2005. An efficient numerical scheme for precise time integration of a diffusion–dissolution/precipitation chemical system. Math. Comput. 75 (253), 209–222.

Fathi, S.J., Austad, T., Strand, S., 2011. Water-based enhanced oil recovery (EOR) by "Smart Water": optimal ionic composition for EOR in carbonates. Energy Fuels 25, 5173–5179.

Gledhill, D.K., Morse, J.W., 2006. Calcite dissolution kinetics in Na–Ca–Mg–Cl brines. Geochim. Cosmochim. Acta 70, 5802–5813.

Green, D.W., Willhite, G.P., 1998. Enhanced Oil Recovery, SPE Textbook Series, vol. 6. Society of Petroleum Engineers (Chapter 3).

Heggheim, T., Madland, M.V., Risnes, R., Austad, T., 2005. A chemical induced enhanced weakening of chalk by seawater. J. Pet. Sci. Eng. 46, 171–184.

Helgeson, H., Kirkham, D., et al., 1981. Theoretical prediction of the thermodynamic behaviour of aqueous electrolytes by high pressure and temperatures; IV. Am. J. Sci. 281, 1249–1516.

Hiorth, A., Cathles, L.M., Kolnes, J., Vikane, O., Lohne, A., Madland, M.V., 2008. A chemical model for the seawater–CO_2–carbonate system – aqueous and surface chemistry, Paper prepared for presentation at the Wettability Conference held in Abu Dhabi, UAE, 27–28 October, 2008.

Hiorth, A., Cathles, L.M., Madland, M.V., 2010. The impact of pore water chemistry on carbonate surface charge and oil wettability. Transp. Porous Media 85, 1–21.

Hilhorst, F., van der Hout, R., Peletier, L.A., 1996. The fast reaction limit for a reaction–diffusion system. J. Math. Anal. Appl. 199, 349–373.

Hilhorst, F., van der Hout, R., Peletier, L.A., 2000. Nonlinear diffusion in the presence of fast reaction. Nonlinear Anal. 41, 803–823.

Knabner, P., van Duijn, C.J., Hengst, S., 1995. An analysis of crystal dissolution fronts in flows through porous media. Part 1: compatible boundary conditions. Adv. Water Resour. 18 (3), 171–185.

Korsnes, R.I., Madland, M.V., Austad, T., Haver, S., Rœsland, G., 2008. The effects of temperature on the water weakening of chalk by seawater. J. Pet. Sci. Eng. 60 (3-4), 183–193.

Langmuir, D., 1997. Aqueous Environmental Geochemistry. Prentice Hall.

Lasaga, A.C., 1998. Kinetic Theory in the Earth Sciences. Princeton Series in Geochemistry. Princeton University Press.

LeVeque, R.J., 2002. Finite Volume Methods for Hyperbolic Problems. Cambridge Texts in Applied Mathematics, Berlin.

Madland, M.V., Finsnes, A., Alkafadgi, A., Risnes, R., Austad, T., 2006. The influence of CO_2 gas and carbonate water on the mechanical stability of chalk. J. Pet. Sci. Eng. 51, 149–168.

Madland, M.V., Hiorth, A., Omdal, E., Megawati, M., Hildebrand-Habel, T., Korsnes, R.I., Evje, S., Cathles, L.M., 2011. Chemical alterations induced by rock–fluid interactions when injecting brines in high porosity chalks. Transp. Porous Media 87, 679–702.

Morse, J.W., Arvidson, R.S., 2002. The dissolution kinetics of major sedimentary carbonate minerals. Earth Sci. Rev. 58, 51–84.

Oelkers, E., Schott, J. (Eds.), 1996. Reactive transport in porous media. Reviews in Mineralogy & Geochemistry, vol 34.

Oelkers, E., Schott, J. (Eds.), 2009. Thermodynamics and kinetics of water–rock interaction. Reviews in Mineralogy & Geochemistry, vol. 70.

Parkhurst, D.L., Appelo, C.A.J., 1999. User's guide to PHREEQC (version 2) – a computer program for speciation, batch-reaction, one-dimensional transport, and inverse geochemical calculations. U.S. Geological Survey Water-Resources Investigations Report 99–4259, pp. 312.

Pawell, A., Krannich, K.-D., 1996. Dissolution effects in transport in porous media. SIAM J. Appl. Math. 56 (1), 89–118.

Pokrovsky, O.S., Golubev, S.V., Schott, J., Castillo, A., 2009. Calcite, dolomite and magnesite dissolution kinetics in aqueous solutions at acid to circumneutral pH, 25 to 150 °C and 1 to 55 atm pCO_2: new constraints on CO_2 sequestration in sedimentary basins. Chem. Geol. 265, 20–32.

Rider, M., 2002. The Geological Interpretation of Well Logs, 2nd ed. Rider-French Consulting Ltd. (Chapter 6).

Rubin, J., 1983. Transport of reacting solutes in porous media: relation between mathematical nature of the problem formulation and chemical nature of reactions. Water Resour. Res. 19 (5), 1231–1252.

Standnes, D.C., Austad, T., 2000. Wettability alteration in chalk 2. Mechanism for wettability alteration from oil-wet to water-wet using surfactants. J. Pet. Sci. Eng. 28, 123–143.

Standnes, D.C., Austad, T., 2003. Wettability alteration in carbonate interaction between cationic surfactant and carboxylates as a key factor in wettability alteration from oil-wet to water-wet conditions. Colloids Surf. A Physicochem. Eng. Aspects 216, 243–259.

Steefel, C.I., Lasaga, A.C., 1994. A coupled model for transport of multiple chemical species and kinetic precipitation/dissolution reactions with application to reactive flow in single phase hydrothermal systems. Am. J. Sci. 294, 529–592.

Strand, S., Standnes, D.C., Austad, T., 2000. Spontaneous imbibition of aqueous surfactant solutions into neutral to oil-wet carbonate cores: effects of brine salinity and composition. Energy Fuels 17, 1133–1144.

Strand, S., Hœgnesen, E.J., Austad, T., 2006. Wettability alteration of carbonates—effects of potential determining ions (Ca^{2+} and SO_4^{2-}) and temperature. Colloids Surf. A Physicochem. Eng. Aspects 275, 1–10.

Strand, S., Standnes, D.C., Austad, T., 2007. New wettability test for chalk based on chromatographic separation of SCN^- and SO_4^{2-}. J. Pet. Sci. Eng. 52, 187–197.

Strang, G., 1968. On the construction and comparison of difference schemes. SIAM J. Numer. Anal. 5, 506–517.

Willis, C., Rubin, J., 1987. Transport of reacting solutes subject to a moving dissolution boundary: numerical methods and solutions. Water Resour. Res. 23 (8), 1561–1574.

Yu, L., Evje, S., Fjelde, I., Kleppe, H., Kaarstad, T., Skjaeveland, S.M., 2008. Modelling of wettability alteration processes in carbonate oil reservoirs. Networks Heterogeneous Media 3 (1), 149–183.

Zhang, P., Austad, T., 2006. Wettability and oil recovery from carbonates: effects of temperature and potential determining ions. Colloids Surf. A Physicochem. Eng. Aspects 279, 179–187.

Zhang, P., Tweheyo, M.T., Austad, T., 2007. Wettability alteration and improved oil recovery by spontaneous imbibition of seawater into chalk: impact of the potential determining ions Ca^{2+}, Mg^{2+}, and SO_4^{2-}. Colloids Surf. A Physicochem. Eng. Aspects 301, 199–208.